Title
Comparative analysis of SOFC–GT freight locomotive fueled by natural gas and diesel with onboard reformation

Journal
Applied Energy, 148(C)

ISSN
0306-2619

Authors
Martinez, Andrew S
Brouwer, Jacob
Samuelsen, G Scott

Publication Date
2015-06-01

DOI
10.1016/j.apenergy.2015.01.093

Applied Energy 148 (2015) 421–438

Contents lists available at ScienceDirect

Applied Energy

journal homepage: www.elsevier.com/locate/apenergy

Comparative analysis of SOFC–GT freight locomotive fueled by natural gas and diesel with onboard reformation

Andrew S. Martinez, Jacob Brouwer, G. Scott Samuelsen *

National Fuel Cell Research Center, University of California, Irvine, CA 92697-3550, United States

HIGHLIGHTS

- Dynamic simulation model of an SOFC–GT-powered locomotive with onboard reformation.
- A diesel-powered SOFC–GT locomotive is predicted with 52.2% efficiency.
- A natural gas-powered SOFC–GT locomotive is predicted with 60% efficiency.
- The saving in CO_2/NO_x is 30.3%/97.7% and 53.8%/97.7% respectively.
- The natural gas-powered SOFC–GT locomotive has distinctive advantages.

ARTICLE INFO

Article history:
Received 11 November 2014
Received in revised form 19 January 2015
Accepted 20 January 2015
Available online 4 April 2015

Keywords:
Fuel cells
Locomotives
SOFC gas turbine hybrid
Diesel fuel
Natural gas

ABSTRACT

Due to increasing awareness of the deleterious environmental and health effects of diesel combustion emissions, major regulatory action and policy measures are focused on reducing emissions from diesel engines. Freight operations, including rail-based freight transportation, have received special attention as an industry where major change can be affected, especially in neighborhoods located near operations centers. A FORTRAN-based dynamic simulation model of an SOFC–GT (Solid Oxide Fuel Cell–Gas Turbine) system from a prior feasibility study has been adapted to analyze system operation along a representative but demanding route in southern California. In previous simulations with the model, the basic operational feasibility of the system has been demonstrated as well as the in-service operation for pre-reformed fuels. In the current study, the analysis is extended to include reformation of two fuels (diesel and natural gas) onboard the locomotive and analyses of system efficiency, fuel consumption, CO_2 emission, and NO_x emission that can be attained through careful thermal integration of the reformer unit. Route-averaged fuel-to-wheels system efficiencies of 60% and 52% are predicted for natural gas and diesel fuel, respectively. Additionally, SOFC–GT operation could provide (1) a reduction approaching 98% in NO_x for both fuels; (2) a 54% savings in CO_2 for operation on natural gas; and (3) a 30% CO_2 reduction for operation on diesel fuel compared to state-of-the-art locomotive technology. These gains may be offset by design challenges, especially for the diesel case, due to the requirement for large volumes of water to support the reformation process even for medium-length freight hauling trips.

1. Introduction

The combustion of diesel fuel drives the transportation of freight, a major sector of the United States and California economies. It has been estimated that more than $1 out of every $10 of the national Gross Domestic Product is related to the transportation of goods [1]. In 2007, the total value of all goods shipped was approximately $11.7 trillion dollars, generated by nearly 12.5 billion tons of goods. These goods traveled over an extensive network of railways, highways, and pipelines, and onboard ships and airplanes for a total movement of 3.34 billion ton-miles, averaging 619 miles per individual shipment [2]. In 2010, the transportation sector generated approximately 9.22 million jobs, accounting for 7.1% of the total US employment [3]. Approximately 27% of these were jobs directly from the various sectors that handle the transportation of freight in particular. The Ports of Los Angeles and Long Beach alone handled 70 million metric tons of freight, valued at $364 billion, and generated $5.1 billion of tax revenue and 1.1 million jobs for California in 2008; the national effect was $21.5 billion and 3.3 million jobs [4,5].

However, any economic benefits of the industry are tempered by the associated environmental impacts. These impacts are especially taxing to the air quality near ports or rail transportation

* Corresponding author. Tel.: +1 (949)824 5468.
E-mail address: gss@uci.edu (G.S. Samuelsen).

http://dx.doi.org/10.1016/j.apenergy.2015.01.093
0306-2619/

hubs, such as those present in the southern California region. Greenhouse gases and criteria pollutants have long been of concern; recently, the emission of diesel-related particulate matter has received much attention due to its high potential for serious health effects. For example, port-related activities accounted for approximately 1760 tons of PM emissions in 2002; this is 21% of the entire South Coast Air Basin (SoCAB) emission signature. Of that, approximately 18 tons were contributed by the operation of in-port locomotives. This, however, is not a true representation of the share from all locomotives as in-port locomotives refers to those that operate solely within the port [6]. It is estimated that the emissions from the port-related sources in the SoCAB in 2008 were as shown in Table 1 [5].

The California Air Resources Board (CARB) estimated that in 2008, the emission of pollutants from freight-haul locomotives, in particular, were as listed in Table 2 [7]. (TOG refers to Total Organic Compounds and ROG refers to Reactive Organic Compounds.) With the exception of NO_x, the share of criteria pollutant emissions by freight-haul compared to statewide emissions is quite low. As a result, it may initially seem that (1) freight-haul locomotives do not contribute substantially to the overall emissions, and (2) NO_x may be the greatest concern associated with freight-haul locomotives. However, locomotives spend a large amount of operating time at major freight centers, including ports, rail yards, and sorting centers. It is at these locations that locomotive emissions represent a significant concern.

For example, the BNSF rail yard in San Bernardino was the subject of a recent health risk assessment [8]. Within the areas closest to the rail yard, the additional risk for respiratory cancer was greater than 500 in a million; the average was 986 in a million. This is in addition to an estimated background risk of only 1000 in a million, effectively doubling the cancer risk. This affected 3780 people living in neighborhoods in this region. Within one mile of the facility, the additional risk was still greater than 100 in a million. 35,800 residents were thus found to have an increased cancer risk between 100 and 500 in a million, increasing their cancer risk by 10–50% above the background impact. Incremental cancer risks of at least 25 in a million were found to be in effect even four miles away from the rail yard, affecting 152,280 residents [8]. Localized impacts are thus a major concern when considering locomotive environmental and health impacts.

The development of fuel cell-based solutions to this problem has been markedly slower than the development of fuel cells for passenger vehicles. Indeed, industry attention is focused on diesel combustion engines, with the GE EVO Series locomotive being the most advanced representative [9]. Given how thoroughly the diesel engine has penetrated the locomotive market, the development of strategies to improve diesel engine performance is a logical first step. However, fuel cells and other new technologies could provide the opportunity to leverage investments in other fields and thereby provide significant emissions reduction and efficiency improvement for the evolving railway system. Thus, the fuel cell has been identified as having the potential to replace the entire diesel and electric power system for a locomotive [10].

This type of fuel cell application has been studied since the 1980s, especially in the context of use for the Canadian rail system [11–13]. Due to the early development stage and lack of mass-production for many of the fuel cell types at the time, it was often concluded that while capable, fuel cell systems were simply too expensive to be practical [11,14,15]. The overall assessment of fuel cell-based locomotives has somewhat varied; however, there have been positive indications from previous detailed investigations. These investigations span the passenger, freight, switcher, mining, and even military locomotive applications [16–21]. However, in these studies and developments, the investigators and designers have looked primarily at Proton Exchange Membrane (PEM) fuel cell systems. This choice inherently raises questions of hydrogen availability, which are not particularly addressed. There has also been some concern about the specific power of the fuel cell system, due to the limited space available on a locomotive. The Solid Oxide Fuel Cell (SOFC) is, in principle, an able alternative in addressing the concerns raised by the application of PEMFCs [22,23].

Aside from these early assessments, the literature contains little in-depth analysis of the SOFC locomotive. Other than this work and the two prior related feasibility analyses [24,25], assessment of SOFC technology for locomotives has only recently appeared in a pair of academic pursuits. In a study of a long-haul SOFC locomotive, Schroeder and Majumdar [26] concluded that such a system could feasibly be produced. However, the packaging of the system on the locomotive platform would require major engineering effort and the cost benefits of the SOFC over a traditional ICE are barely enough to justify the effort. In a more detailed system dynamic analysis, Guo et al. [27] simulated the performance of a hybrid SOFC-battery-ultra-capacitor system for a switcher locomotive. Based on a simplified lump, equivalent-circuit model, and with the SOFC run in an essentially base-loading mode (thereby not responsible for any of the system power dynamics), the authors reported a positive outlook for satisfying the electrical demands of the application.

The current investigation builds upon the simplified system analyses developed in the two prior feasibility analyses [24,25]. In those works, a conceptual system design for an SOFC–gas turbine hybrid system was assessed based on its steady-state and in-service operational capability. However, these analyses were performed using simplified system designs that did not model, in detail, the conversion of the primary fuel (natural gas or diesel) into the reformate streams required to power the locomotive. The primary goal of the current work is to assess the system performance, accounting for the requirements of fossil fuel reformation and the possibilities for thermal integration and heat recovery to support this process.

Diesel fuel is a ubiquitous energy carrier for many transportation applications throughout the world. It is estimated that as many as 1.4 billion barrels of distillate fuel (a general classification for the various grades of diesel fuel utilized in transportation and

Table 1
Port operations-related emissions from POLA/LB in 2008.

	PM_{10}	$PM_{2.5}$	NO_x	SO_x	CO	HC	CO_2 equivalent
2008 Emission (Tons)	857	738	15,253	3804	4052	837	1,045,061
Share of SoCAB	9%		5%	24%	–	–	–

Table 2
Estimated emission of criteria pollutants by freight haul locomotives in California.

	TOG	ROG	CO	NO_x	SO_x	PM	PM_{10}	$PM_{2.5}$
Emissions (tons/day)	12.78	10.69	33.10	123.65	0.79	3.96	3.96	3.64
Percent of state mobile sources	1.02	0.942	0.366	4.50	0.483	2.43	2.48	3.21
Percent of all state sources	0.222	0.483	0.292	3.85	0.284	0.106	0.187	0.573

stationary applications combined) were consumed in 2008 in the United States alone [28]. In spite of the environmental impact, the diesel engine has been adopted for the advantages of its cost, maintenance cycle, thermal efficiency, and power density.

As environmental regulations become increasingly stringent, it has become of interest to find a way to utilize this diesel fuel in a cleaner and more efficient way. While combustion post-treatment remains an industry focus, much research effort has recently been spent on attempting to design high-temperature SOFC power systems that can operate on diesel [29–33]. Given that state-of-the-art SOFC technology cannot directly oxidize the diesel itself, it has also become of great interest to understand and improve the process of diesel reformation. Recent research has focused on catalysts that improve reforming efficiency, reduce the concentration of complex hydrocarbons in the reformate, and reduce the propensity for coking within the reformer. This latter effect is a concern within the SOFC as well, and much work is currently underway to replace SOFC nickel-based catalysts with materials less active at promoting carbon deposition [34–38].

The major goal of the reformation of diesel fuel for use in SOFC applications is to convert the original fuel into a stream rich in hydrogen and carbon monoxide, both of which act as fuels in the anode compartment. Although other methods for diesel reformation have been developed, auto-thermal reformation (ATR) is often the preferred reaction route due to its balance of thermal requirements, use of air to break down complex hydrocarbons, and desirable product concentrations. In an overall sense, idealized ATR can be represented as in the reaction shown in Eqs. (1)–(4).

Steam reforming:

$$C_nH_m + nH_2O \rightarrow nCO + (n + 0.5m)H_2 \quad (1)$$

Partial oxidation:

$$C_nH_m + 0.5nO_2 \rightarrow nCO + 0.5mH_2 \quad (2)$$

Water–gas shift:

$$CO + H_2O \leftrightarrow CO_2 + H_2 \quad (3)$$

Total:

$$C_nH_m + AnO_2 + SnH_2O \rightarrow nCO_2 + \left(\frac{m}{2} + 2n(1 - A)\right)H_2 + (S - 2(1 - AnH))_2O \quad (4)$$

In Eq. (4), S is the steam-to-carbon ratio, S/C, and 2A is the oxygen to carbon ratio, O/C. It is important to note that Eq. (4) is the summation of the steam reformation and partial oxidation reactions, with consideration for the water–gas shift that inevitably occurs along with reformation at typical operating temperatures. These reactions typically include both homogeneous reactions as well as heterogeneous interactions with a supported catalyst that often includes nickel. As with the SOFC, research efforts have been underway to replace the nickel in order to reduce coke formation and deposition in diesel reformation reactors.

Typically, diesel fuel is a mixture of hydrocarbons with carbon numbers ranging from 6 to 24, with the relative weight percent of each constituent varying among diesel sources [39]; it is the combustion properties that define a fuel as diesel. However, diesel fuel is often replaced in both experimental and modeling studies by a surrogate of roughly the same carbon-to-hydrogen ratio; tetradecane, $C_{14}H_{30}$, is one of the more commonly-cited surrogates in studies of reformation mechanisms and simulation.

In an effort to predict reformation reactor performance and understand the overall process of diesel ATR, many researchers have developed model kinetic reaction mechanisms that describe the full process of ATR in varying degrees of detail. Comprehensive models are based on elementary reaction kinetics, emphasizing the roles of short-lived radical species, adsorption reactions and adsorbed species, and the availability of sites of reactions [40–44]. These models typically involve thousands of reactions and species, and attempt to describe not only the evolution of final products but also the full suite of short-lived (e.g., radical) species that may be influential in directing the reaction progress.

By contrast, studies involving system-wide analyses require simplified models that capture the major features of these comprehensive mechanisms but save computational time by reducing complexity [45,46]. Because this type of mechanism is often used in practical applications, examples spanning various degrees of complexity have been discussed in the literature. Some of the simplest models consider only Eq. (4) in combination with the individual steam reformation, partial oxidation, and water–gas shift mechanisms shown in the reactions of Eqs. (1)–(3). Alternatively, when investigators have not been concerned with dynamic performance expectations, Gibbs reactors have been utilized [47–50]. For steady-state analysis, this simplicity may provide sufficient accuracy and detail.

However, when one becomes concerned with accurately simulating the composition of exhaust species and the full electrochemical and possible post-reformation pathways within the fuel cell itself, this coarse level of detail is not sufficient. Additionally, a thermodynamic analysis will be an ideal one, not accounting for the effects of incomplete reactions due to slow catalyzed kinetics. This consideration can have major consequences on dynamic operation.

The current study incorporates a simplified, yet detailed chemical kinetic model, which includes 24 reactions based upon phenomenological observations of experimental tetradecane ATR over a conventional catalyst [51]. This mechanism differs from the comprehensive ones in that the total number of intermediate hydrocarbons, and radical species is greatly reduced. For many measures, the predicted concentrations matched previous experimental data; however, the expected accuracy is limited [51]. This exemplifies the tradeoff that simplified, phenomenological reaction mechanisms make: the mechanism requires less computational effort, but provides only an approximate prediction for certain conditions.

Against the backdrop of these research and development efforts, a large gap remains in a thorough dynamic system analysis for an SOFC system, including consideration of the fuel processing requirement, applicable to long-haul freight application. In addition, research regarding the particular SOFC–GT hybrid cycle used in this application has not yet been undertaken, excepting the previous work upon which this investigation is built. Given the potential benefits in system efficiency, power density, and overall system integration, the need for such an investigation is evident.

2. Modeling methodology to characterize dynamic operation

Prior investigations utilizing the FORTRAN-based simulation model of this study have discussed the full details of the model structure, methodology, physics, chemistry and electrochemistry included, numerical methods, and convergence criteria [24,25]. In the current study, these details are largely the same, but certain additions and alterations have been introduced in order to accommodate the integrated dynamic simulation of the reformer module and the effects that such integration has on performance and model structure. Figs. 1 and 2 show the system schematics for the natural gas and diesel fueled systems, respectively. The major difference between the two is the type of the reformer; the natural gas case employed a steam-methane reformer (SMR) while the diesel case was modeled with an autothermal reformer (ATR). The operation of these reformer designs dictates that each has differing requirements for inlet reactant feeds, as illustrated. Moreover, by comparing the system schematic of this work to those presented

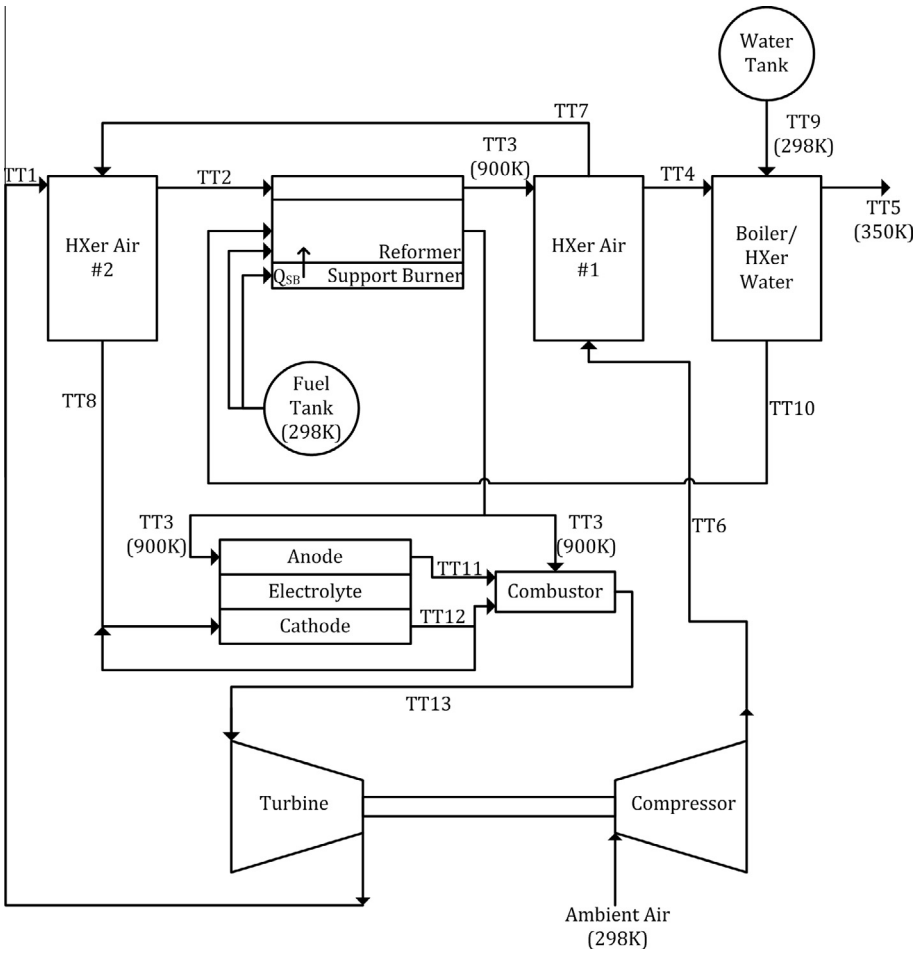

Fig. 1. Natural gas system design with thermally-integrated SMR reformer.

in the prior feasibility study, it is clear that the systems considered here are more complex. System integration and operation requirements addressed with the current model include the dynamics of fuel processing and preheating of the fuel and air for the fuel cell.

For the current systems, air enters through the compressor of the gas turbine subsystem while fuel and water are drawn from onboard reservoirs. Water is vaporized and preheated in a boiler while the air flows through a preheating network supported by system exhaust and reformer waste heat and, if necessary, partially siphoned off to support the operation of the reformer (ATR). Reformer products are directed towards the fuel cell stack anode and the auxiliary combustor (the division of which is managed via controller logic) and the preheated air is directed towards the SOFC stack cathode. Following electrochemical reaction in the SOFC, the depleted fuel and air streams are combined with the fuel sent directly to the combustor and undergo complete reaction. The exhaust of the combustor is directed to the turbine, which is connected to a generator (not shown) to produce electricity. The exhaust of the turbine passes through the heat recovery loop, supporting the prior air and water preheating. A support burner is assumed to be integrated with the reformer in order to provide additional thermal energy as needed to dynamically maintain the reformer temperature at 900 K. This heat is denoted in the schematic as Q_{SB} and is assumed to be provided by burning non-reformed fuel.

Solutions of many of the states depicted in the two systems (denoted as TT1 through TT13) are described in [25]. In particular, the states surrounding the fuel cell, combustor, and turbo-machinery are described. However, the states around the reformer and within the heat recovery system were newly developed for this investigation and their solution integrated into the overall model methodology. In the current investigation, the system solution began with the compressor to determine state TT6. Utilizing the exhaust composition of the previous time step and the assumption of thermal equilibrium between the reformer body and all its outlet flows to describe state TT3, the heat exchange in HXer Air #1 was resolved to determine outlet states TT4 and TT7. Again utilizing the turbine outlet condition of the previous time step for state TT1, HXer Air #2 was similarly analyzed to determine states TT2 and TT8. In addition, with TT4, TT9, and TT5 known, the outlet of the boiler and steam preheater (TT10) was determined. This process was modeled as two distinct steps, with phase change calculated prior to vapor preheat. Thus, the water vapor only absorbed the amount of heat released between states TT4 and TT5 of the system exhaust, less the heat of vaporization. The two air preheaters were modeled as counterflow plate-fin heat exchangers with quasi-two-dimensional resolution, as previously described.

Aside from the heat recovery network, there are three major hardware subsystems within the overall model: the fuel reformer, the SOFC stack, and the turbo-machinery (consisting of compressor, turbine, plenum, and shaft). The compressor and turbine were modeled via interpolation on generalized performance maps obtained from the GasTurb software [52] and scaled to maximum and design operating parameters matching the published data for the Solar Turbines Saturn 20. This turbine's operating parameters were chosen as representative of the limits of the turbo-machinery map due its close match to the required turbine subsystem power of 1000 kW, accounting for a 50% derate in developed power (thus

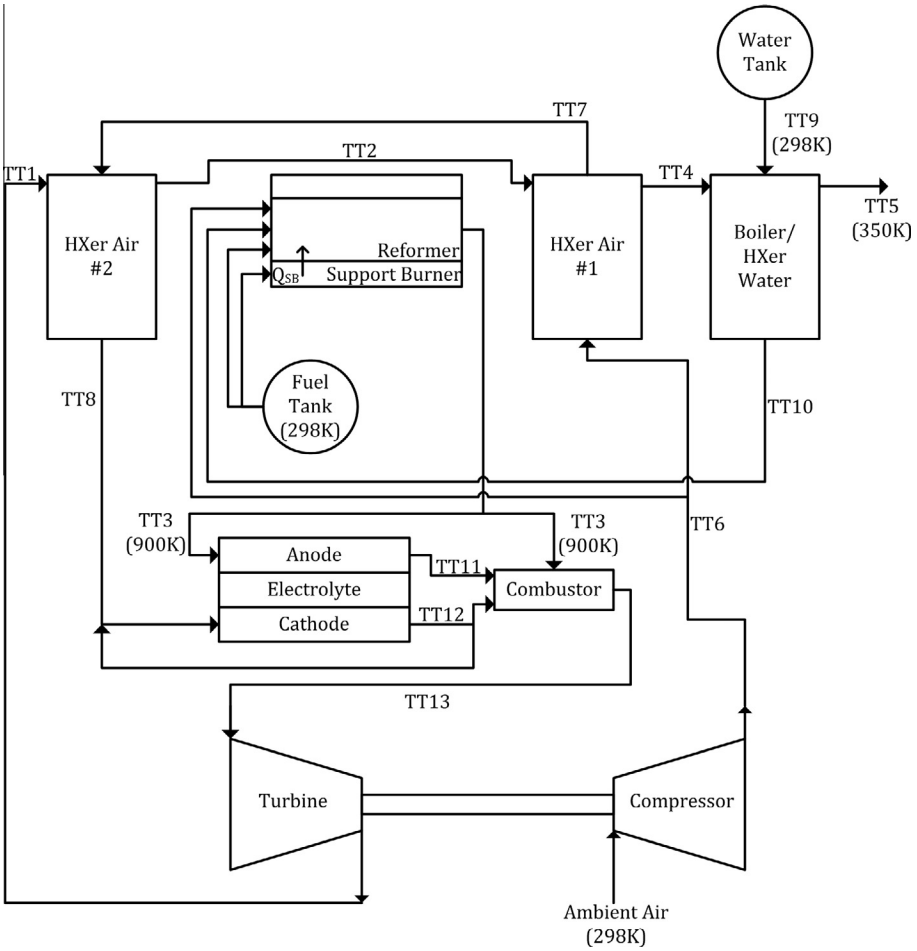

Fig. 2. Diesel system design with thermally-integrated ATR reformer.

the turbo-machinery is expected to provide ~500 kW at design point operation). In order to approximate the dynamics of pressure changes within the volume of the compressor itself, a plenum was simulated just after the compressor, thereby slightly dampening the dynamic mass flow response to changes in pressure ratio, as in Eq. (5).

$$\frac{dP}{dt} = (\dot{N}_{In} - \dot{N}_{Out})\frac{RT}{V} \tag{5}$$

where P is the pressure, $\dot{N}$ is the molar flowrate, R is the universal gas constant, T is the temperature, and V is the plenum volume. In model execution, the outlet flow rate was the unknown; thus, Eq. (5) was solved for this parameter with the rate of change in pressure known from the prior solution and current guess of compressor operating point.

Dynamic determination of the operating point on each map was carried out by interpolating against the coordinates of pressure ratio and shaft speed to calculate the component efficiency and mass flow rate. During solution of the system, the shaft speed for a given time step was determined in the previous system solution via a torque balance around the shaft:

$$\frac{dN_{GT}}{dt} = \frac{1}{J_{Shaft} \cdot N_{GT}} \cdot (P_T - P_C - P_{Load} - P_{Loss}) \tag{6}$$

where N_{GT} is the shaft speed, J_{Shaft} is its rotational inertia, and P_T, P_C, P_{Load}, and P_{Loss} are the power produced by the turbine, and consumed by the compressor, the generator load, and the frictional losses (assumed to be 5% of the balance between turbine and compressor), respectively. By contrast, the pressure ratio was a guessed parameter. Utilizing a guessed pressure ratio and known shaft speed would yield a mass flow rate at the turbine. Looking at the system diagrams in Figs. 1 and 2, it is clear that solution of the combustor outlet state would also yield a mass flow rate at the same point in the system. Determination of the proper pressure ratio, and thus overall system convergence, was determined by a mass conservation check at this point. If the guessed pressure ratio did not yield a mass flow rate from the turbine map that matched the combustor's outlet flow (to within a tunable precision), then the system solution was not converged, and a new pressure ratio was determined and the entire system solved again.

By contrast, the SOFC model was based on first principles for each of the participating physics, and was structured according to a quasi-2-dimensional spatially and temporally resolved model of a single channel within the co-flow SOFC. As Fig. 3 demonstrates, it was assumed that the SOFC stack contained one centrally-located cell whose performance was representative of the average over all cells in the stack. Moreover, within that cell, the centrally-located channel (comprised of anode gas channel, tri-layer, cathode gas channel, and current collector) had a performance representative of all channels across the cell. This channel was then isolated and divided into nodes along the direction of flow of the reactant gases. Each node was then assumed to be small enough in physical size and simulated with a small enough time step that it could be treated as a perfectly-stirred reactor. Thus, the solution for the state of the gases within a node could also be treated as the state of those same gases exiting the node and thus entering the next node in sequence. This allowed solution of the SOFC nodes

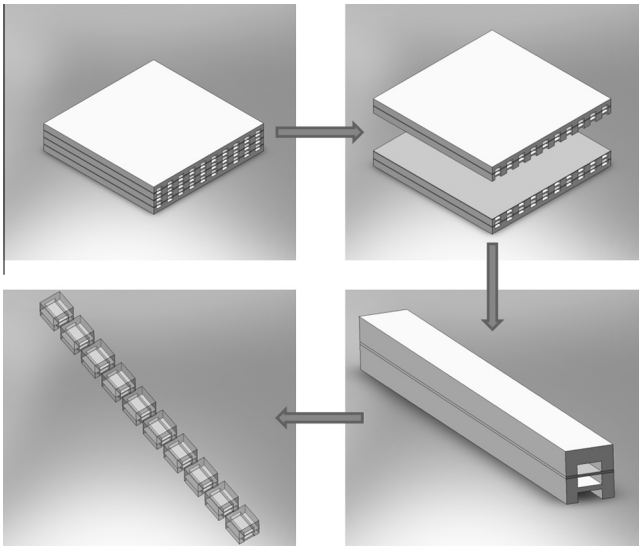

Fig. 3. SOFC simplification to modeled control volumes.

to proceed sequentially from inlet to node 1, 2, 3... until it reached node 10, where the SOFC outlet condition could be resolved.

The major physical models incorporated in the SOFC subsystem related to thermodynamics, conservation of momentum, reformation reaction kinetics, electrochemistry, conservation of mass, and heat transfer. Each of these models, previously developed and described [24,25], were solved in the sequence shown in Fig. 4. In execution, the inlet and initial conditions were utilized to calculate the changes in a node state dictated by each of these physics. However, given the interdependence of the node state variables (mole fractions, pressure, temperature, molar flow rate, and current density) and each of these physics with each other, a convergence criterion had to be utilized to ensure the self-consistency of the node solution. This criterion was based on the solution of the current density, which was directly calculated by the thermodynamics and model, but dependent on all the physics incorporated. It was assumed that the voltage (dictated by an external system controller) was required to be constant across the length of the SOFC channel. The voltage, E_1, was determined according to Eq. (7), where E_N is the Nernst potential (shown in Eq. (8)), and the various η are loss terms, dependent on the state of the gases and the electrolyte as well as the current density. With E_1 known, the current density can be solved via an implicit root-finding method. Calculating the current density based on the inlet and initial state of the node and comparing this to the value calculated after the changes in a time step are accounted for allows for a convergence criterion that ensures the constant-voltage assumption is maintained. In Eq. (8), E_0 is the reversible potential for a hydrogen cell, T_{Tri} is the temperature of the SOFC tri-layer, p is the partial pressure, n is the number of electrons involved in the reaction (2 for hydrogen electrochemistry), and F is Faraday's constant. This SOFC subsystem model was previously validated against a widely-referenced standard in the fuel cell literature [24].

$$E_1 = E_N - \eta_{Activation,A} - \eta_{Activation,C} - \eta_{Concentration,A} - \eta_{Concentration,C} - \eta_{Ohmic} \quad (7)$$

$$E_N = E_0 + \frac{RT_{Tri}}{nF} \ln\left(\frac{p_{H_2} \cdot p_{O_2}^{\frac{1}{2}}}{p_{H_2O}}\right) \quad (8)$$

The reformer model and method varied between the two systems, although there were some similarities. As presented, both reformers were modeled to maintain a constant temperature of

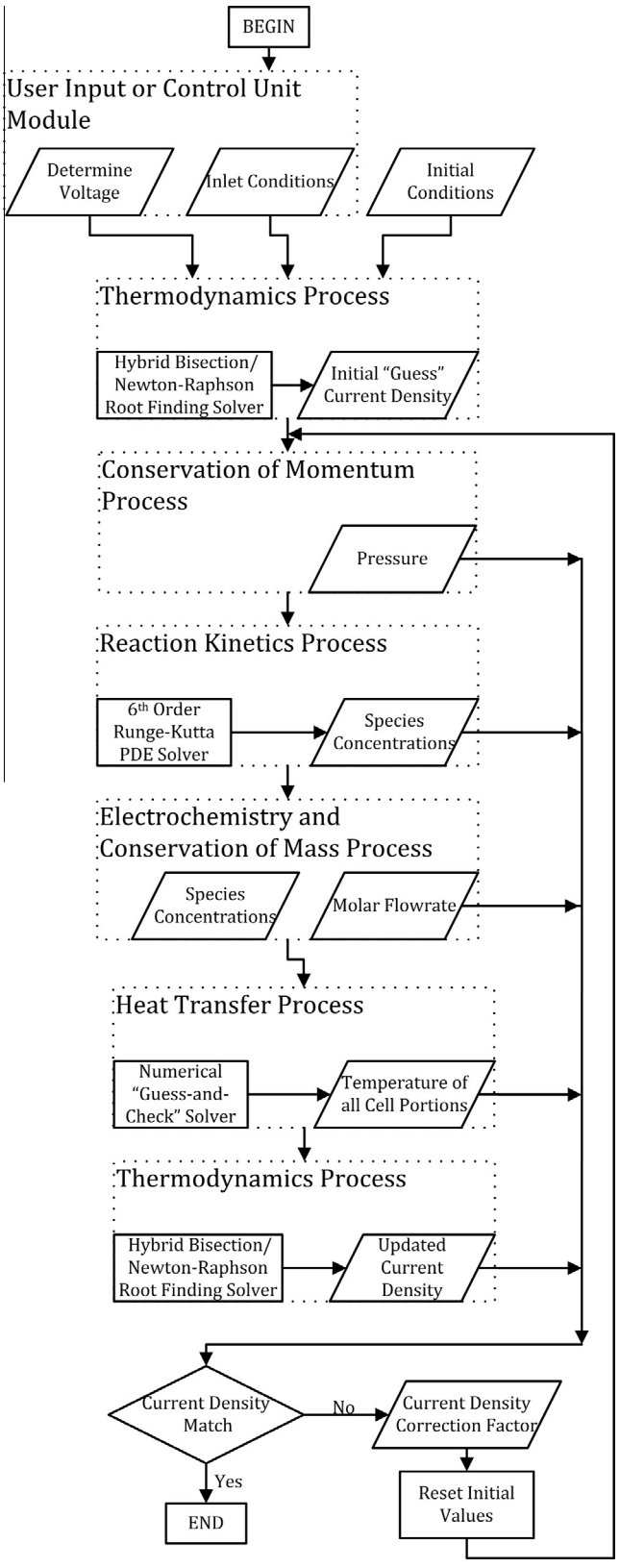

Fig. 4. SOFC node solution process and convergence criterion.

900 K, which was assumed to also be the temperature of reaction and controlled by an integrated burner. In addition, both models incorporated conservation of mass and were modeled as constant temperature and pressure processes. The total volume of the reformer in each case (utilized to determine total residence time and

thermal mass) was estimated as 3.87 m^3. In the case of the natural gas-fueled system, the only reactions considered were related to steam-methane reformation and water gas-shift:

(1) $CH_4 + H_2O \leftrightarrow CO + 3H_2$ (9)

(2) $CO + H_2O \leftrightarrow CO_2 + H_2$ (10)

(3) $CH_4 + 2H_2O \leftrightarrow CO_2 + 4H_2$ (11)

Only these reactions were modeled in the SOFC reformation kinetics model for both fuel cases. The simplicity of these reactions allowed dynamic solution with a 6th-Order Runge–Kutta method. By contrast, the diesel reformer model incorporated the kinetics presented by Dorazio and Castaldi [51], which includes 24 reactions and 17 species (see Appendix A for full reaction set), based on the reformation of tetradecane. This system of reactions is not only more complex, but the timescales of the various reactions result in an extremely stiff set of descriptive Ordinary Differential Equations. Thus, the freeware Double-Precision Livermore Solver for ODE's (DLSODE) was incorporated for fast and efficient solution of the set of stiff differential equations describing the rates of change of species concentrations of Eq. (12).

$$\frac{\partial y_i}{\partial t} = \sum_{j,forward} k_j A_{j,i} \left(\prod_m y_m^{A_{j,m}} \right) - \sum_{j,backward} k_j A_{j,i} \left(\prod_m y_m^{A_{j,m}} \right) \quad (12)$$

Eq. (12) is written in the form assuming that species i (with corresponding concentration y_i) is a product in the forward direction of a reversible reaction. The variable k represents the reaction rate of reaction j, limited to only reactions involving species i, $A_{j,x}$ is the stoichiometric coefficient for species x in reaction j, and m represents only the species involved in reaction j, which includes species i.

The integration of this numerical method was first verified by replicating the results of the Dorazio and Castaldi work. This required modifying the reformer to incorporate an energy balance and modifying and incorporating DLSODE to accommodate this changing parameter of the reaction rate expressions. In addition, given the complexity of the calculations, the number of time steps, and the small concentrations of some of the species, machine error had to be counterbalanced by adjustable parameters. Small (on the order of 0.01% or smaller) adjustments based on mass conservation were incorporated into the final solution in every reformation time step (each of which was 100 times smaller than the overall system time step) by applying the following corrections:

$$\dot{N}^*_{Node} = \frac{P \cdot V}{R_u \cdot T} \quad (13)$$

$$\dot{N}_{Node} = \dot{N}^*_{Node} \frac{M_{Pre-Ref}}{M_{Post-Ref}} \quad (14)$$

$$y_i = y_i^* \frac{1}{\sum_i y_i^*} \quad (15)$$

where $\dot{N}_{Node}$ is the finalized molar flow rate, y_i is the finalized mole fraction of species i, $M_{Pre\text{-}Ref}$ and $M_{Post\text{-}Ref}$ are the total mass pre- and post-reformation, and y_i^* is the molar fraction post-reformation.

When modeling the full system with the reformer integrated, the O/C and S/C ratios were chosen to be 0.73 and 3.0, respectively. The selection of these values was aided by the use of the NASA Chemical Equilibrium with Applications Freeware equilibrium estimator to find an inlet O/C and S/C ratio that allowed for an autothermal condition. This was determined by manipulating O/C and S/C to find a near-zero difference in reactant and product enthalpies during a constant temperature and pressure reaction. Candidate values were obtained from CEA and then fine-tuned through pilot investigations with simulation of the Dorazio and Castaldi mechanism to find ratios that provided a slightly exothermic reaction at fuel flow rates required for rated power.

In addition to the physical models within the power system, the system controller, train kinematics, and locomotive notching logic models were incorporated into the system simulation. These were all implemented as presented in the prior use of the model [24,25]. Furthermore, the simulations completed in this work were carried out for servicing the route previously described: the train begins in the port of Los Angeles/Long Beach, travels through Los Angeles, Orange, and Riverside Counties then into San Bernardino County, where it scales the peak of the Cajon Pass before traveling nearly consistently downhill into Barstow, its final destination. Cajon Pass is known for challenging grades (up to 3%) and large volumes of rail traffic; the Pass serves as a "gateway" for trains traveling between southern California and destinations east of San Bernardino. In 2010, a study of rail traffic in southern California estimated that the pass was traversed by approximately 82 freight trains per day [53]. By comparison, the other major rail lines west of the pass in the study area experienced an average of only 44 freight trains per day.

The performance of the two SOFC–GT systems was then compared to calculated performance of a modern locomotive diesel combustion engine. For the two SOFC–GT systems, exhaust carbon dioxide was calculated directly from model results of the state of the system exhaust. Exhaust NO_x emissions were estimated based upon prior observation from a pilot SOFC–GT system, at 0.04 kg/MW h (0.0298 g/bhp h) [54]. Efficiency for each system was calculated according to Eq. (16).

$$\eta_{Sys} = \frac{P_{SOFC} + P_{Turb} - P_{Blow}}{\dot{LHV}_{SOFC+Turb} + \dot{LHV}_{Q_{SB}}} \quad (16)$$

where P_{SOFC} is the power produced by the SOFC stack, P_{Turb} is the net power provided by the turbo-machinery to the generator, P_{Blow} is the power consumed by the blower recirculating air around the SOCFC cathode, and the denominator is the Lower Heating Value (LHV) of the fuel entering the reformer to support the SOFC, the pre-turbine, auxiliary combustor, and the reformer support burner. Water consumption was tracked during runtime with the assumptions of a S/C ratio of 2.5 for the natural gas case and 3.0 for the diesel case (with an O/C ratio of 0.46). For the diesel combustion engine, fuel consumption (and therefore efficiency) was based on scaling the power curve of the Caterpillar 3516B engine by the ratio of the required 3.5 MW to its rated 1678 kW [55]. Carbon Dioxide emissions were then based on an EPA estimate of 10,217 g CO_2/gal diesel, as in the prior investigation [56]. Finally, NO_x estimates for this engine were not available; rather, it was assumed that the EPA Tier 4 emission standard for new locomotives (1.3 g/bhp h) [56] applied.

3. Verification of diesel reformer model

The mechanism for diesel reformation utilized in this investigation had previously been developed by Dorazio and Castaldi [51] with the aid of KINTECUS. [57] Although the KINTECUS file and results data were provided by the previous authors, neither KINTECUS itself nor its solvers could be integrated into the FORTRAN environment. For this reason, the diesel reformer model was developed in this work as previously described. A verification test, replicating the conditions of the previous work's simulations, was carried out to ensure proper application of the reformation chemical kinetic mechanism and to study the sensitivity of final solution state to the time step of the DLSODE solver. For this verification and further use of the model, the relative and absolute

tolerance of the DLSODE solver were set to 1.E−12, as was the tolerance for the solution of the energy equation implemented to solve for the gas temperature. In addition, the option to allow the solver to estimate the Jacobian of the set of ODE's was implemented.

The current FORTRAN model was therefore operated under these settings and with the initial conditions matching case "A" outlined in the previous work [51]. The conditions from this case are as shown in Table 3. The results for many of the species of interest in this case are presented in Fig. 5, for a simulation step size of 1.e−7 s. It can be seen from the figure that the trends for all of the species concentrations are quite smooth, and show an overall consumption of the main fuel species, $C_{14}H_{30}$, and the main oxidant, O_2, with a corresponding rise in the activity of the water–gas shift reaction and the production of hydrogen as well as the small hydrocarbon species. Interestingly, propylene (C_3H_6) can be seen to begin a net consumption towards the end of the 20 ms simulation. Although it is somewhat consumed during the process, the water concentration does remain relatively unchanged throughout the course of the reformation, most likely due to its high initial concentration compared to the other active species. Comparison to a similar figure in the original work shows a close match in the species' concentration profiles.

When viewed as a whole, the final product composition of the reformate appears to be near equilibrium for some species (H_2O, O_2, CO_2, CH_4). However, the remainder of the species are still undergoing relatively significant changes at the end of the 20 ms simulation. Thus, the system does not appear to be quite at equilibrium. This has an effect on the whole system model as the reformate outlet stream is also the input for the SOFC and combustor modules, thereby having an effect on the physics simulated within those subsystems. Additionally, the results presented in Fig. 5 are for a specific inlet condition; in the dynamic simulation, the inlet condition to the reformer and the support burner requirement could vary due to dynamic changes in the various system temperatures for streams and processes interacting with the reformer.

A number of other parameters were tracked during the execution of the model in order to ensure that all the physics were properly solved. For example, since the reformation model essentially simulates a perfectly-stirred reactor with no additional inlet or outlet points, mass must be conserved at all times during the simulation. Tracking of total mass ensured this conservation was maintained. Similarly, tracking of the total mole fraction ensured that, at all time steps, the value did not deviate from unity.

Satisfaction of these conservation conditions was aided by the previously-mentioned correction factors for total mass and mole fraction. If the model is constrained to maintain a constant mass, and the gases in the model are assumed to be ideal, then at all times the Ideal Gas Law must hold:

$$PV = mR_uT \tag{17}$$

Inherent to the formulation of the rates of change in species concentration shown in Eq. (12) is the assumption that the system is at constant volume. Given that the volume is therefore fixed, as is the universal gas constant, then it must be expected that the pressure will need to change proportionally to temperature in order to maintain constant mass. Thus, the main algorithm in this validation also calculated the pressure at the end of every time step, according to Eq. (17).

Table 3
Reformation baseline case initial conditions.

Parameter	Value
Temperature (K)	1173
Pressure (kPa)	101.325
Molar flowrate (kmol/s)	1.2167e−6
H_2O mole fraction	0.25
O_2 mole fraction	0.05
N_2 mole fraction	0.69
$C_{14}H_{30}$ mole fraction	0.01

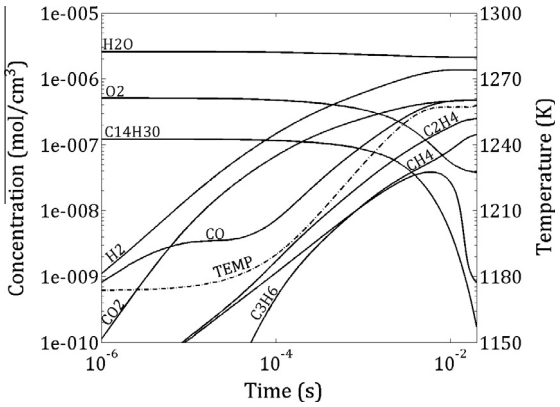

Fig. 5. Modeled diesel reformation products as a function of residence time.

The effect of this constraint can be seen in Fig. 6a. During the course of the reformation process, the pressure rises relative to the temperature, by a total of approximately 22%. Comparison of Figs. 5 and 6 show the clear relationship between the two state variables. In addition, given that mass is conserved, but species concentrations are not conserved, the total number of moles must also vary during reformation, as shown in panel b of Fig. 6. By considering all of these features, the results of the FORTRAN reformation model are self-consistent and considered to accurately predict the dynamic changes in the state of the reformate stream during reformation.

Fig. 7 provides more details of the direct comparison between the species concentrations predicted in this work and the original work [51] which developed the reformation mechanism. It should be noted that for these results, the total simulation time was 20 ms for the current model and 18 ms for the previous work. (Exact values for the previous work were provided by personal communication with the authors.) As can be seen from the figures, the agreement is acceptable between the predicted species concentration values from the current and previous works. In particular, the main oxidant and fuel species, shown in Fig. 7a, match particularly well as do the small hydrocarbon species, shown in Fig. 7c.

The greatest discrepancy in species concentrations is associated with the water–gas shift reaction (H_2, CO, and CO_2), as can be seen in Fig. 7b. However, the disagreement is not large, especially in the context of comparing complex chemical kinetic models, and agreement amongst all species near the end of the simulated time is reasonable, indicating that while the system does not reach equilibrium in either model, both models well predict an approach to a similar equilibrium condition. It should also be noted that the shapes of the trends match very well; the trend for the development of carbon monoxide during execution time in particular exhibits some interesting characteristics, with its multiple inflection points. This implies that there are multiple reaction paths that affect the evolution of this species, each of which may be dominant during a different portion of time in the reaction set evolution. Indeed, by careful examination of all the trends, it seems that water–gas shift may at first be the dominant reaction in carbon monoxide evolution, with the diesel and hydrocarbon oxidizing reactions taking a more active role after approximately 5 ms. The fact that both the previous and the current models predict this sort of complex interaction between reactions is a positive indication of a close match in the underlying physics of the models.

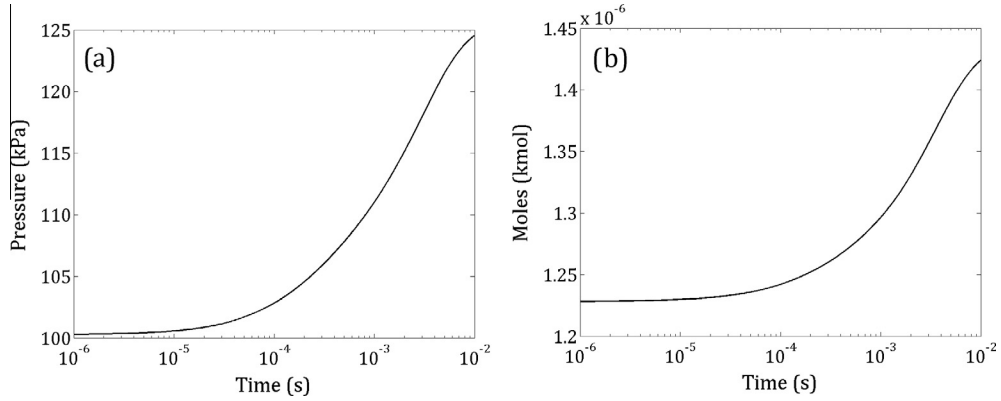

Fig. 6. Rise in pressure and moles during diesel reformation as a function of residence time.

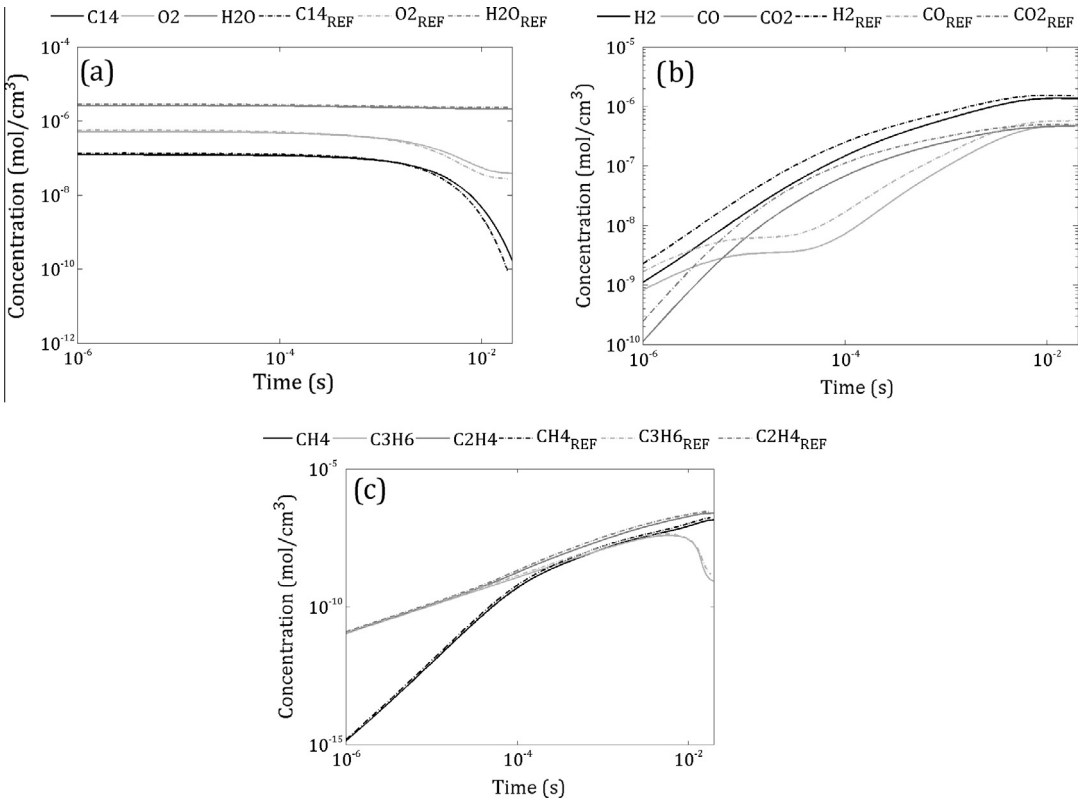

Fig. 7. Comparison of modeled and reference diesel reformation productions as a function of residence time.

Interestingly, in spite of the close match between species concentrations for the two models, the prediction of system temperature in the current model did vary significantly from the previously-reported value. A comparison of the two temperature evolutions is presented in Fig. 8. The discrepancy grows as the reactions progress, ending with a total difference of approximately 40 K. However, note that the temperature solution from the KINTECUS model is not smooth; rather, it has a step-wise characteristic, with time steps becoming shorter during times of greater temperature change. This implies that the temperature solution in the KINTECUS method is executed according to an adaptive time step and that this time step is different from the one used to calculate species concentrations, perhaps in an effort to minimize computational effort. However, since the temperature is maintained at a constant value for some discrete amount of time rather than smoothly changing during that period, it may end up altering the calculated rates of reaction, all of which depend heavily upon system temperature.

Additionally, as Eq. (17) shows, there is a close relationship between the system temperature and pressure for the Ideal Gas assumption; unfortunately, the KINTECUS model does not report pressure, so there is the possibility that some of the discrepancy in temperature and species concentrations may be reflected in differences in pressure that cannot be investigated. Finally, it is worth noting that the source reformation model was developed with and verified against prior experimental test data, as discussed in the original work [51]. Thus, the current diesel reformation model's implementation is likely in similar agreement with the experimental results.

With this reformer kinetic model verification complete, a sensitivity analysis was carried out to evaluate the effect of varying time steps on the final species concentrations and gas temperature

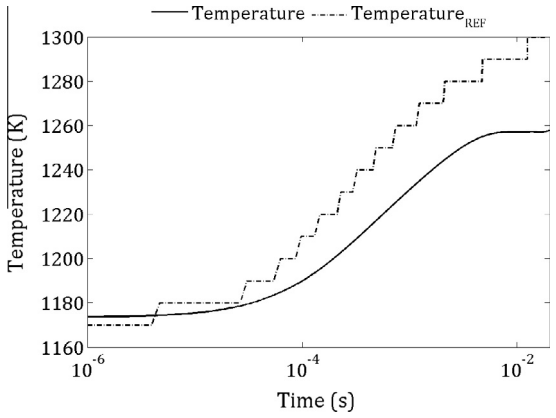

Fig. 8. Comparison of modeled and reference temperature during diesel reformation as a function of residence time.

Table 4
Errors in modeled diesel reformation products compared to reference for multiple solution time steps.

	Model 1e−3 s (%)	Model 1e−4 s (%)	Model 1e−7 s (%)	Model 1e−9 s (%)
C_{14}	**125.5**	60.5	60.9	60.3
C_2H_4	−8.6	−6.9	−6.8	−6.8
C_3H_6	−28.9	**−33.2**	−33.1	−33.1
CH_4	**−17.6**	−15.3	−15.2	−15.2
H_2O	−9.3	**−9.4**	−9.3	−9.3
H_2	−9.7	−10.4	**−10.5**	**−10.5**
CO	−15.6	−16.6	**−16.8**	**−16.8**
O_2	16.3	26.7	**28.2**	**28.2**
CO_2	−5.9	**−6.0**	**−6.0**	**−6.0**
Temp ∗ 1e−9	−3.3	**−3.4**	**−3.4**	**−3.4**

at 20 ms. Thus, the LSODE-based model was run additional times with time steps of 1.E−9, 1.E−4, and 1.E−3 s. The final species concentrations for the nine species previously presented and the temperature were then compared to the values reported in the previous work. The relative errors in all these measures at all time steps are presented in Table 4, with the largest errors in each species and temperature in bold. Note that for time steps of 1.E−4 and smaller, all errors are small, especially compared to the error in the previous work from the cited experimental results [51]. Thus, by utilizing a time step of 1.E−4 s, the diesel reformation model was able to run sufficiently fast enough for smooth integration into the overall system model while providing a satisfactorily high accuracy.

4. System modeling results and discussion

4.1. Natural gas-fed system

In prior use of the full SOFC–GT system model, the overall performance was analyzed for steady-state rated operation, simple dynamic step changes in power demand, and systems operating along the Cajon Pass route, but fueled by hydrogen and hydrocarbon reformate streams that were assumed to be generated off-board. Throughout the completion of these simulations, the system model, and in particular its control structure and tuning, was altered from its original form. The current investigation models the system performance with the final system control methodology and tuning presented in the prior simulations of the train's operating route [24,25]. In addition, just as in the previous simulations, the system was first simulated until a steady-state condition at rated power was obtained. This was then used as the initial state for the dynamic simulation of the train operation as it completed the Cajon Pass route. Therefore, the major change in this work, compared to prior simulations, is the integrated simulation of the new heat recovery and fuel processing system, potentially leading to fuel composition entering the SOFC and auxiliary combustor that can vary dynamically.

Thus, in operation many of the major features, especially of the system control, were found to be very similar to the off-board reformer case in their overall behavior, but exhibited much shorter settling times and much less pronounced transient overshoots. Overall, the dynamic responses more closely mirror the previous hydrogen cases than the prior natural gas reformate case. Fig. 9 provides an overview of the natural gas-fed system's operation during the route. As can be seen in panel a, the overall train's motion was largely unaffected by the change in the fueling method, with the train velocity remaining between the maximum and minimum velocities for almost the entirety of the route. As in the previous work, the velocity was well-maintained while simultaneously adhering to safety-based constraints, such as lower average speed on downhill portions. This behavior is very similar to observations from the prior fuel cases and may be expected given the previous agreement between the differing fuel compositions already examined. Contributing to this was the result that although the fuel composition was dynamically resolved, the reformer's outlet species composition was relatively constant due to the relatively simplicity of the natural gas reforming mechanism and its fast kinetic rates.

Fig. 9b shows that the system power transients were relatively smooth and characterized by very short settling times and a small number of oscillations, though the magnitude of initial overshoots appeared large for large step changes in system power. This behavior was smoother than the transients observed in the model with the fuel reformed off-board of the locomotive. This improved dynamic performance may be due at least in part to the fact that in the current system, the fuel temperature was consistently maintained at 900 K by control of the reformer temperature. In the prior design, the fuel was preheated via a heat exchanger, which was subject to all of the dynamic changes in performance throughout the system, including heat generation upstream, changes in air flow rate, etc. This may be a realizable control benefit due to the typical thermal mass and rapid combustion control response characteristics of the fuel processing system.

Fig. 9c shows the contrast in the dynamically-calculated system efficiency between the SOFC–GT case (inclusive of the reformer) and the conventional diesel engine case. Note that the diesel combustion – electric case performance is not based upon a physical dynamic model, as described previously. The SOFC–GT system is significantly more efficient at all times excluding some brief transients; however, as noted in prior work, the advantage of the SOFC–GT system decreases as total system power decreases. Finally, from Fig. 9d, it can be seen that for much of the time, the reformer support burner fuel flow was either low or completely off. In fact, aside from some transient requirements, the flow appears to only be required at full power, when approximately $6.5 \times 10^{-5} \frac{\text{kmol}}{\text{s}}$ are required, which represents $52.2 \frac{\text{kJ}}{\text{s}}$ (compared to $6.5 \times 10^{-3} \frac{\text{kmol}}{\text{s}}$ consumed for production of power). Thus, even at its most taxing operation, the reformer burner fuel requirement is a small portion of the total system fuel requirement and therefore did not present a great loss to overall efficiency.

Profiles of the instantaneous and cumulative CO_2 and NO_x emissions from both the SOFC–GT system and the diesel-electric system are provided in Fig. 10. It should be noted that these values are on a per-locomotive basis. Again, the diesel engine emissions are only provided as estimates and are based upon the dynamic power

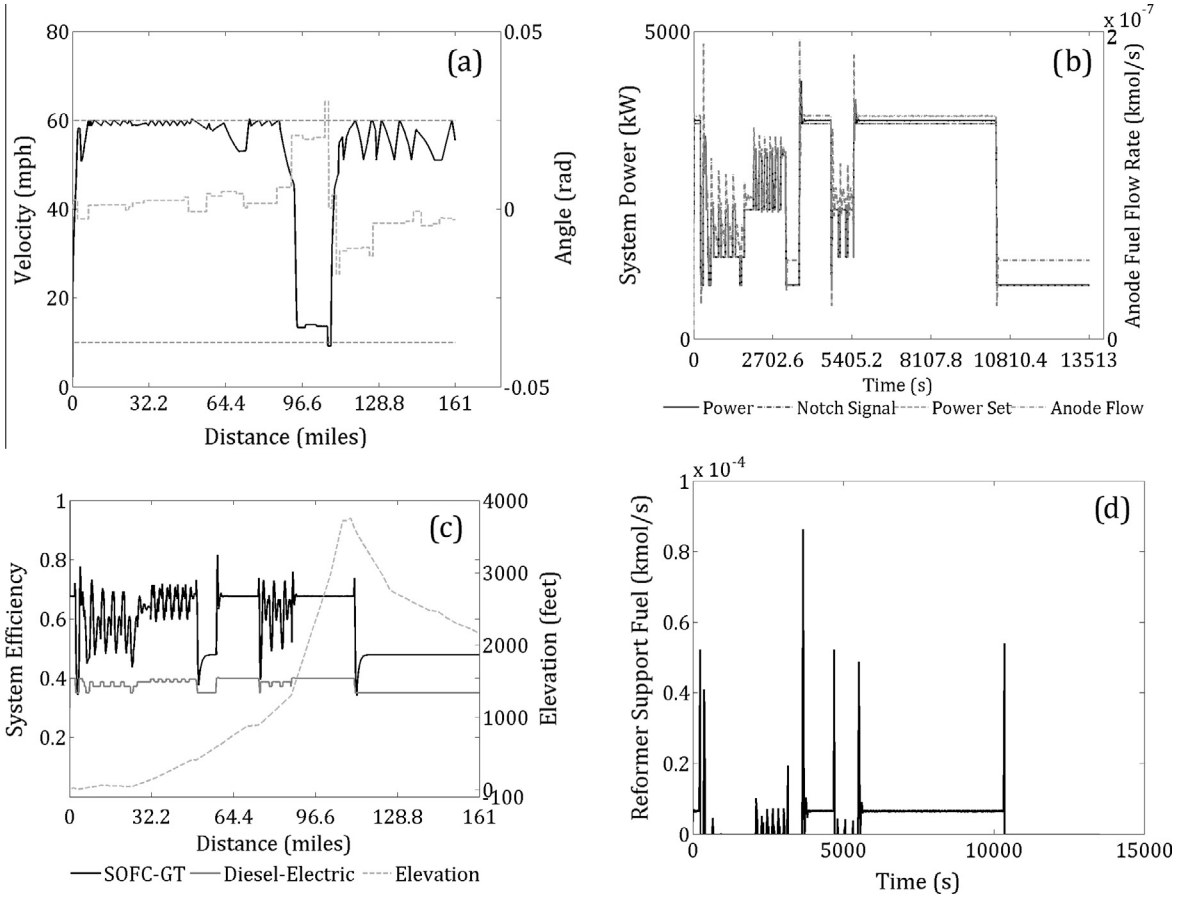

Fig. 9. System performance of thermally-integrated natural gas SOFC–GT locomotive.

requested of the SOFC–GT system. As would be expected from the requirements of fuel consumption to meet higher power demands, in general, both emission rates increase as the grade of the geography increases. Moreover, changes in notch setting are clearly visible in the emission rate data, especially for the diesel-electric case.

At all times during the simulation, the SOFC–GT system was able to provide significant savings in the production of both CO_2 and NO_x; the former being directly related to the higher efficiency and the latter owing more to the limited maximum temperatures and separate fuel and oxidant streams of the SOFC–GT compared to the diesel combustion case. The final comparison of engine emissions at the end of the service route is provided in Table 5. Clearly, the potential for savings in NO_x, in particular, is quite substantial and could be of great value in a geographic area with a propensity for smog formation. However, the potential reduction in CO_2 emissions is also quite large, with more than half of the emissions from the train removed by use of an SOFC–GT power system.

Total water consumption (all of which was required simply to support the SMR reactions) was found to be 730 gallons for the entire Cajon Pass trip. Current locomotives do carry water tanks, which are needed to provide cooling for the diesel reciprocating engines. Considering the GE EVO locomotive as representative, the typical onboard water tank capacity is only 450 gallons [9]. However, the EVO also carries an additional 450 gallons of lubricating oil to support the engine's function. In the SOFC–GT, the SOFC does not require any lubricating oil. In addition, according to Kawasaki, their GPS 1250 (1 MW) requires only 0.08 $\frac{L}{h}$ of oil at rated power [58]. Thus, for the Cajon Pass trip, the maximum lubricating oil consumption for the GT portion may be only 0.08 gallons. This then leaves the potential for the lubricating oil tank to be all but removed in order to make room for a larger water tank to support the SOFC–GT system's reformation needs.

Finally, Table 6 provides a comparison in efficiency between the cases of an off-board reformer and an onboard reformer. When looking at the raw data from the two simulations (100% reformer efficiency for the off-board case), at low power settings, there is apparently not any benefit to including the reformer onboard even potentially presenting an overall cost to the system. Since this is when no additional fuel is flowing to the reformer to support its thermal requirements, it is more likely that the composition of the fuel at this lower power setting may be slightly less advantageous than the assumed reformate for the off-board case. On the other hand, at high power, and overall, the onboard reformer case does provide a few points in efficiency gain. However, these results do not account for the thermodynamic efficiency of the off-board natural gas reformer, only for the thermal load required to heat the fuel prior to the SOFC and combustor. Thus, the overall benefit of including the reformer onboard is potentially much greater. If the SMR reactor is assumed to have an efficiency of 83% (as in prior simulations), then the system efficiency with an off-board reformer drops significantly and the advantage of the onboard thermally-integrated reformer becomes much more apparent, providing a 12-point advantage.

4.2. Diesel-fed system

At the chosen S/C and O/C ratios, representative outlet mole fractions of the onboard reformer were found to be as listed in Table 7, with a total reformer thermodynamic efficiency of 93%

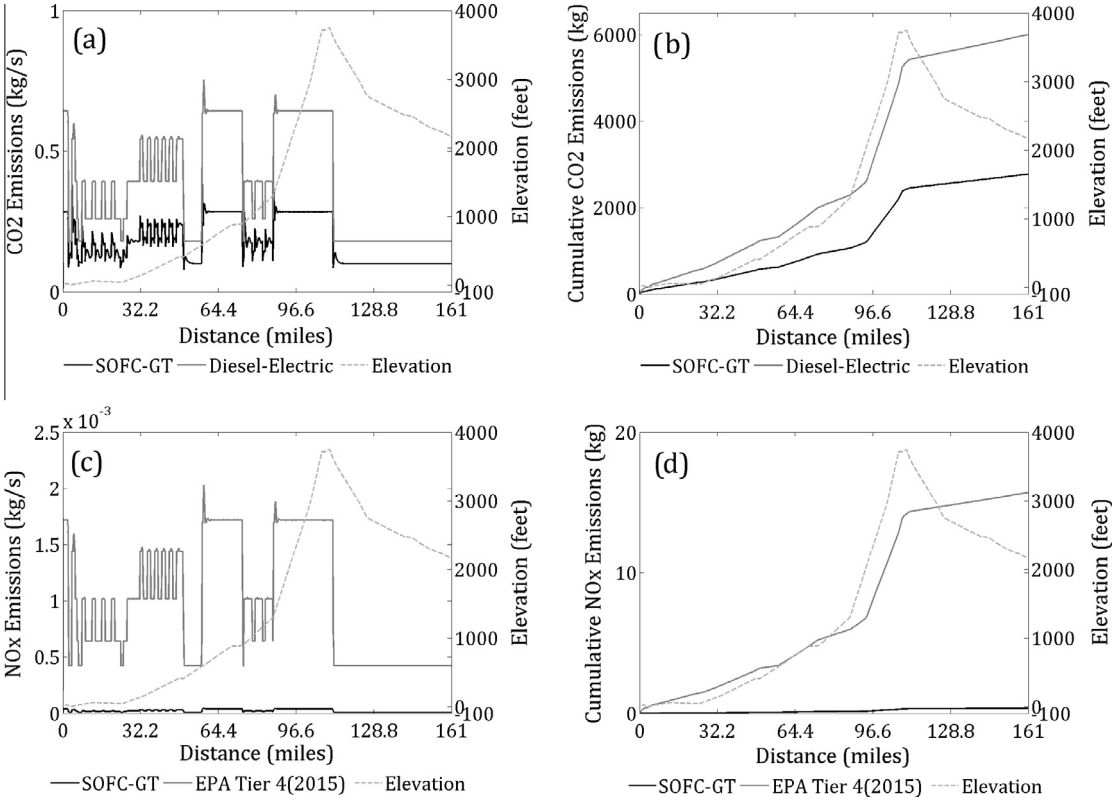

Fig. 10. Comparison of emissions between thermally-integrated natural gas SOFC–GT locomotive and conventional diesel-electric locomotive.

Table 5
Total emissions and savings for thermally-integrated natural gas SOFC–GT locomotive compared to conventional diesel-electric.

System	NO_x (kg)	CO_2 (kg)
Diesel	15.700	5997.1
SOFC–GT	0.3602	2772.2
Savings	97.7%	53.8%

Table 6
Comparison of efficiency of natural gas SOFC–GT locomotive with off-board and on-board reformation.

System	High-power (%)	Low-power (%)	Total (%)
Offboard reformer (100% η reformer)	64	48	58
Offboard reformer (83% η reformer)	53	40	48
Onboard reformer	67	47	60

Table 7
Representative diesel reformer outlet composition.

Species	Mole fraction
H_2	0.2697
CH_4	6.3581E−03
H_2O	0.3547
CO	3.3749E−02
CO_2	0.1040
O_2	1.4531E−03
N_2	0.2218
CH_3	1.8116E−06
C_2H_4	8.2151E−03
C_2H_5	5.7307E−13
C_3H_6	6.2797E−07
C_3H_7	1.1991E−07
C_4H_9	0.0
C_7H_{14}	0.0
C_7H_{16}	0.0
$C_{14}H_{30}$	0.0
OH	6.4592E−10
H	4.8393E−07
C_2H_3	1.3755E−08

and tetradecane conversion efficiency near 100%. Compared to the diesel reformate in the off-board reformation case, there is significantly less nitrogen and carbon monoxide and approximately twice as much steam, in addition to the new species included in this model fuel.

The overall response of the train and power system under these conditions is shown in Fig. 11. Panel a makes it immediately clear that under this control scheme, there is a significant concern for the train's motion. Immediately after the crest of the Cajon Pass peak, the train experienced a prolonged overshoot of the maximum speed desired, and reached 73.9 mph. Although the train's operation was shown to subsequently recover from this violation of the maximum speed, this can still present a dangerous situation and may be a greater problem along a route with a more extended steep drop. This behavior prompted an investigation into changes in the power management for this particular system design.

Aside from this issue, in Fig. 11b, it can be seen that in general, the transient behavior of the SOFC–GT is similar to what has previously been observed in the off-board diesel reformate case. There are increased oscillations in controlled and manipulated parameters in this case compared to the natural gas case. In addition, larger changes in power demand generated larger transient spikes, overshooting the change requested. Compared to the previous diesel reformate case, it can be seen that the dynamically changing reformate composition (shown in Fig. 12) also generated more oscillations in system power, indicating a substantial effect of the newly-included chemistry and physics. Fig. 11c shows that in

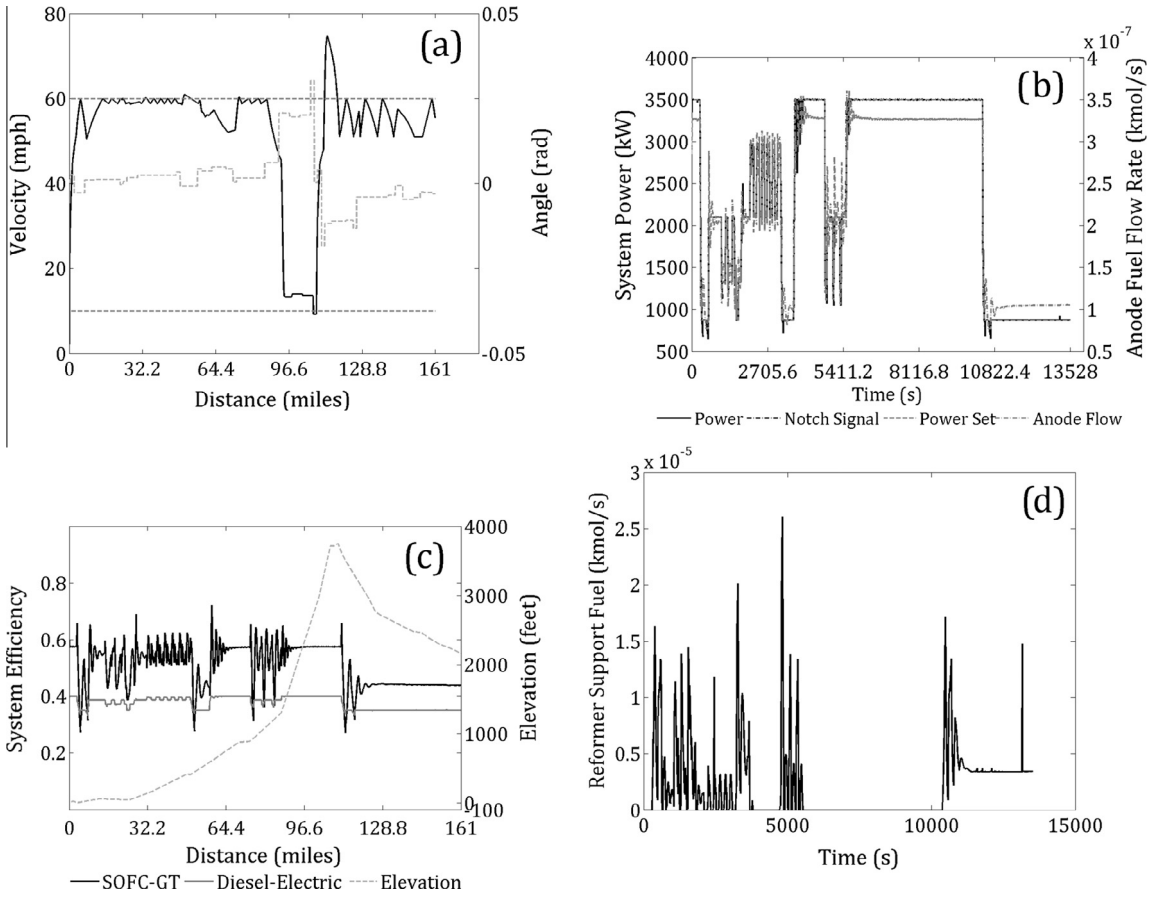

Fig. 11. System performance of thermally-integrated diesel SOFC–GT locomotive.

spite of these difficulties in controlling the train's motion, the system efficiency is quite high, and provides a major advantage over the conventional diesel engine. Finally, Fig. 11d shows that for the ATR reformer, the most strenuous fuel requirements were during dynamics and at low system power; this is in sharp contrast to the SMR case and is likely due to the fundamental differences in thermal requirements for the two reformation processes.

It can be seen from Fig. 11b that the violations of maximum speed roughly coincided with power settings at notches 0 and 1 and an apparent inability to meet system power demand quickly in these states. At these notches, the power delivered by the system required longer settling times to the target, resulting in some short instances of excess power to the wheels. Fig. 13 shows that the timing of these violations also coincided with violations in the maximum anode utilization target. During these times, the controller logic required attention to be focused upon the anode utilization, not allowing system power to be controlled temporarily. Thus, the system developed power is momentarily unable to respond to a decreased demand in power. Therefore, a number of alternative control methods were developed to attempt to address this issue by altering the behavior and priority of the utilization controller, to wit:

(a) Change the maximum utilization to 95% at all notches.
(b) Change the maximum utilization to 95% for notches 0, 1, and 2.
(c) Change the maximum utilization to 95% for notches 0, 1, 2, and 3.
(d) Increase the utilization proportional gain.
(e) Increase the utilization proportional gain and the system power proportional and integral gains.

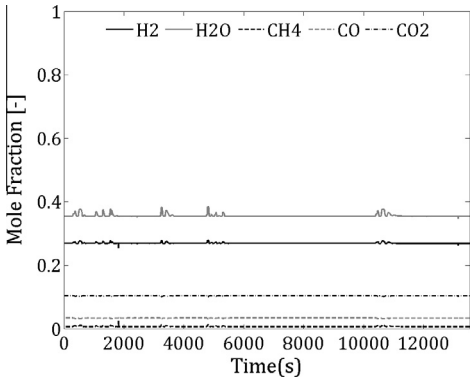

Fig. 12. Diesel reformer outlet composition during Cajon Pass route simulation.

(f) Change the maximum utilization to 95% for notches 0, 1, and 2 and increase the system power integral gain.
(g) Change the utilization target to 82%.
(h) Remove the anode utilization control priority over system power.

None of these attempts were successful at addressing the overspeed issue. While some of these failed due to an inability to control the system (in particular, the SOFC would become deactivated in cases with decreased fuel utilization control priority), even the cases that were able to complete the simulation did not result in a lower maximum speed. While the intent of many of these options was to alleviate the utilization control so that system power control could be enabled more often and provide a better match to

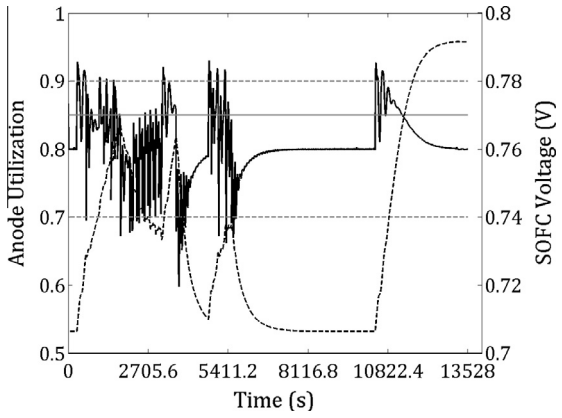

Fig. 13. Anode utilization control during Cajon Pass route simulation of thermally-integrated diesel SOFC–GT locomotive.

system power demand, this alone was not enough to avoid the undesired high velocity. Thus, the next option was to investigate the system power demand curve itself. Fig. 14 displays the notch and braking notch settings for two different cases: the above case with the overspeed and the off-board diesel reformate case where the overspeed did not occur. It is immediately apparent that the notching decisions of the two cases were not equivalent. The key difference is that in the case with the overspeed, there is an extended duration at notch 2, followed by a short duration at notch 1 before finally falling to 0. Thus, for approximately 1 mile, the case with the overspeed provides power to the wheels when the case without the overspeed is actually braking. Although the distance over which this happens is short, the sharp contrast between powering and braking can cause a large impact on overall train speed.

Thus, an attempt was made to restart the Cajon Pass simulation near the peak and force the dynamic notching response exhibited by the case without the overspeed. However, this dynamic was not sustainable with the changing fuel composition modeled in this case, and the system again was not well controlled. The alternative was then to replicate the notch decisions of the case with the overspeed (allowing for the settling time required of the new system), but to shift them backwards to an earlier point in the route. Thus, the notching changes in the overspeed case were forced to begin at a position such that the final drop to notch 0 coincided with the position of the same drop in the case without the overspeed (just over 112 miles). Modeling the notching process in such a way is akin to expanding the logic to allow for the locomotive engineer's intuition and experience, a feature that otherwise cannot be replicated with the mechanistic approach taken in this work.

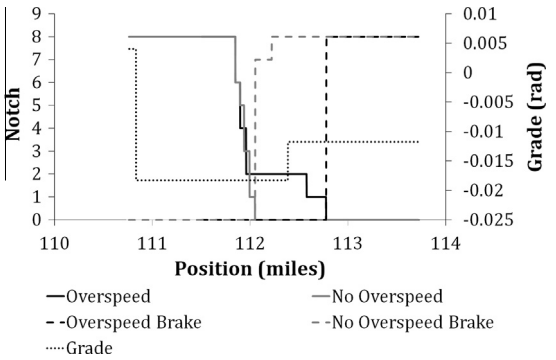

Fig. 14. Comparison of power demand curves between cases with and without overspeed.

Fig. 15 demonstrates that this strategy of merely shifting the notching sequence to an earlier point in the route was successful at avoiding the overspeed issue previously encountered. Moreover, panels c and d of the figure demonstrate that this was achievable even though the system underwent severe transients in anode utilization and system power control, as was the case when the notching shift was not employed. Overall, the data of Fig. 15 demonstrate that the strategy was a success and that in a physical application of the SOFC–GT powered locomotive, the locomotive engineer's intuition and judgment will most likely remain just as critical to successful operation as it currently is when conventional diesel engines are powering the train.

Fig. 16 displays the emissions profiles for this system along the route for CO_2 and NO_x. As with the natural gas case, it can be seen that the diesel–fueled SOFC–GT case provides substantial savings in emission of both of these species. The same assumptions outlined for the natural gas case were utilized for this analysis.

Table 8 displays the total gross and relative savings in these species for the diesel–fueled SOFC–GT compared to the conventional diesel-electric engine. As with the natural gas case with the thermally integrated reformer, nearly 98% of the NO_x is predicted to be avoided. However, for the diesel-fed case, this value includes some inherent uncertainty, as the calculations used as a basis for NO_x production from an SOFC–GT were performed on the basis of a natural gas reformate fuel, not a diesel reformate [54]. Thus, there may be some error introduced by utilizing this production rate. However, temperatures in the combustor were still controlled to be at their minimum possible value at all times in this case; thus, there should not be any substantially increased thermal potential for NO_x production simply due to the change of fuel. By comparison with Table 5, it can also be seen that the CO_2 savings with the diesel fuel is quite a bit less than with the natural gas fuel, at just over 30%.

Likewise, while Table 9 shows that the efficiency of the thermally-integrated diesel case is lower than the natural gas case, there is a similar gain when comparing the thermally-integrated reformer case to the cases when the reformer is assumed to be off-board the train. While overall the natural gas case allowed for a 12-point gain in system efficiency through this thermal integration, the diesel case affords a 7-point gain. This difference is tied to that observed in the amount of CO_2 emissions that can be conserved with operation on each of these fuels. Given the close parity in the comparisons between off-board and onboard reformers in this and the natural gas case, the observations previously made for the natural gas case are equally valid in the diesel case. It should also be noted that the average efficiency predicted for the diesel–fueled case represents a 14-point benefit over the prediction for a conventional diesel engine.

Finally, while the natural gas case found that the total water consumption may be manageable with some re-proportioning of the various onboard fluid tank volumes, the same may not be true for the diesel case. Over the course of the Cajon Pass run, a total of 1311 gallons of water were consumed, nearly double the amount for the natural gas case. Incorporation of a water condenser for the diesel–fueled locomotive may be a requirement in a physical system. Based on the conditions of the exhaust stream at the point TT4 in Fig. 2, a total heat transfer of 3890 kW (equivalent to 1110 tons of refrigeration) would be required to bring the stream to a cold enough temperature for water drop-out. However, as noted for the natural gas case, nearly 900 gallons of water capacity may be available onboard, requiring only 200 gallons (18% of the requirement) to be made up by a water reclamation system. Thus, if it is assumed that only one-fifth of the exhaust must be condensed, then the cooling requirement is only 222 tons. Even this amount of cooling may prove to be a challenge to accommodate onboard the locomotive.

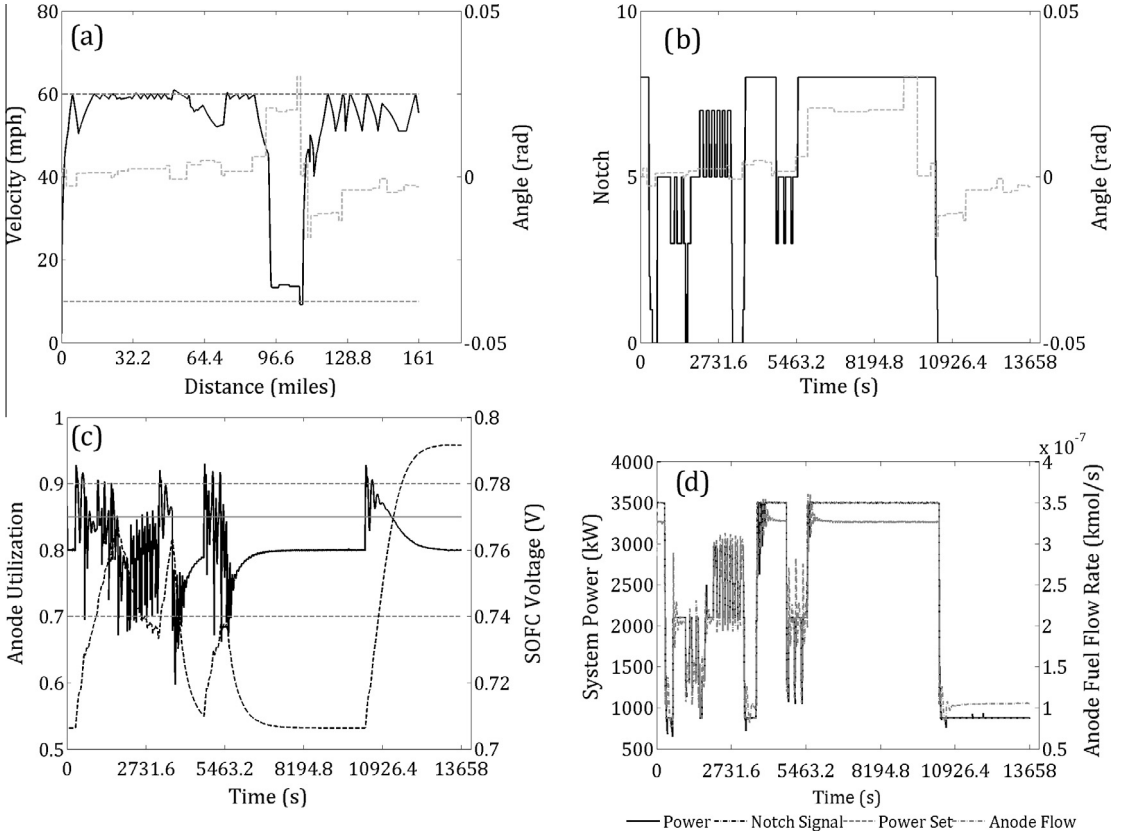

Fig. 15. System performance of thermally-integrated diesel SOFC–GT locomotive with notching shift.

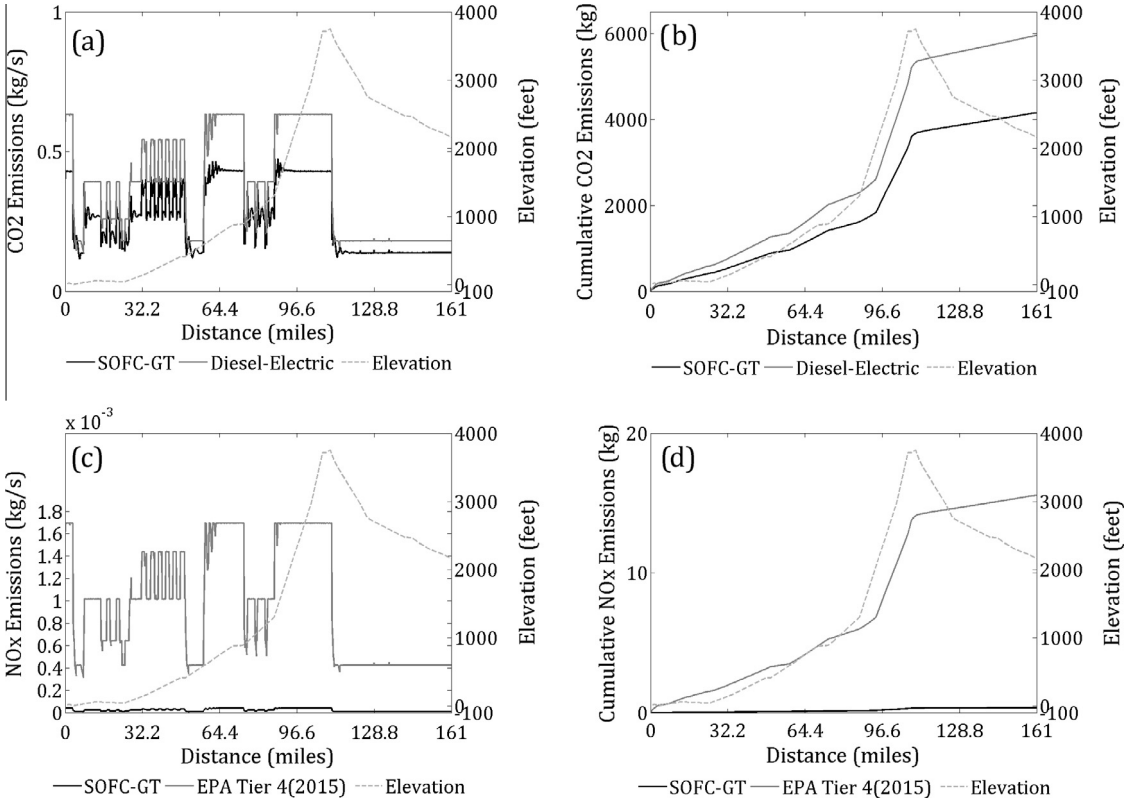

Fig. 16. Comparison of emissions between thermally-integrated diesel SOFC–GT locomotive and conventional diesel-electric locomotive.

Table 8
Total emissions and savings for thermally-integrated diesel SOFC–GT locomotive compared to conventional diesel-electric.

System	NO_x (kg)	CO_2 (kg)
Diesel	15.562	5947.2
SOFC–GT	0.3571	4147.5
Savings	97.7%	30.3%

Table 9
Comparison of efficiency of diesel SOFC–GT locomotive with off-board and on-board reformation.

System	High-power (%)	Low-power (%)	Total (%)
Offboard reformer (100% η reformer)	61	44	55
Offboard reformer (83% η reformer)	51	36	45
Onboard reformer	58	44	52

5. Summary and conclusions

This investigation has advanced the study of the SOFC–GT for locomotive freight transport through dynamic simulation of a system operating on fossil fuels reformed onboard the locomotive. In this configuration, the SOFC–GT meets the application's rigorous performance requirements. Additionally, this capability is achieved while operating at higher efficiency and lower NO_x and CO_2 emissions than a diesel engine. Inclusion of a thermally-integrated onboard reformer enables significantly higher efficiency than systems where the fuel is generated off-board. While a natural gas-powered system exhibits the highest efficiency, a more-readily implemented diesel-powered system also provides a substantial advantage over the conventional reciprocating engine, implying viability as a near-term option. In particular, this investigation finds that:

- A diesel-powered SOFC–GT locomotive exhibits average system efficiency of 52.2%, thereby saving 30.3% of CO_2, and 97.7% of NO_x emissions; however, control of such a system is difficult.

With thermal integration of the diesel autothermal reformer onboard the SOFC–GT locomotive, the average system efficiency can exceed 52%, approximately a 14-point increase over the predicted efficiency for a conventional diesel engine. Half of this gain was found to be due to the onboard thermal integration of the reformer. However, these advantages came at the cost of significant difficulty in system control, due to the dynamically changing composition of the reformate entering the SOFC. In particular, maintenance of safe bounds for anode utilization was consistently found to be difficult for diesel reformate streams.

- Water management may present a significant engineering challenge for diesel-powered SOFC–GT locomotive systems.

Total water consumption during the simulated Cajon Pass route was very large. The requirement of 1100 gallons of water is greater than the water and lubricating oil tanks onboard a typical locomotive combined. This implies that a water condensing and recirculation loop may be required to support the reformation of the fuel. Thus, water management for diesel reformation is expected to be a primary engineering design challenge when developing a physical system for the locomotive application.

- A natural gas-powered SOFC–GT locomotive offers further emissions and fuel savings with average system efficiency of 60%, CO_2 savings of 53.8%, and NO_x savings of 97.7%.

Operation on natural gas was shown to provide highly favorable system performance and substantial savings in emissions and fuel consumption. Performance was characterized by relatively low-amplitude transients with short settling times and no requirement for system control modifications. Moreover, fuel-to-wheels efficiency was found to be higher in the natural gas-fed case than the diesel-fed case. Due to this higher efficiency and the higher hydrogen-to-carbon ratio, CO_2 savings were greater than 50% of a conventional diesel engine's emissions. In particular, there was a 10-point gain in system efficiency attributed to onboard thermal integration of the reformer.

- A natural gas-powered SOFC–GT locomotive is an attractive candidate for next-generation freight trains.

The results of this work and the two previous studies [24,25] demonstrate that the SOFC–GT is a technically viable solution for the demands of the freight locomotive application while significantly reducing emissions of criteria pollutants and greenhouse gases. A natural gas powered SOFC–GT locomotive in particular stands out as an attractive candidate for further design and development. While the diesel fueled option enables the use of existing fueling infrastructure, it imposes difficulties in system operation and design. In addition, diesel fuel may enhance SOFC degradation due to coking in the anode channels (a subject left for future investigations). On the other hand, a hydrogen-fueled system avoids these issues and provides the largest gains in efficiency and emissions but suffers a lack of available fuel resources and infrastructure, implying more favorable viability as a long-term option.

The natural gas-fueled system is an ideal candidate that avoids these difficulties. This work has shown that the natural gas system is not met with operational or design difficulties, with or without a reformer onboard. Moreover, the efficiency demonstrated in the natural gas system varied between ~43% and ~62%, nearly matching the previously-reported range for the hydrogen case of 48–64% [25]. Most importantly, the fuel for this option is currently widely available. Though rail operators may not yet have exclusively-owned infrastructure for natural gas, the fuel is supported by an extensive distribution network in the United States and can be easily obtained. Additionally, recent actions from the industry indicate that natural gas fuel is receiving considerable attention for the near-term future of the industry.

Given the early stage of development of not only the SOFC–GT locomotive application but also SOFC–GT technology itself, it is not yet possible to accurately analyze the full cost associated with implementing the concept. Ongoing research in this area will need to continue as the industry develops. However, as the United States continues to develop its capability for natural gas extraction, the option of utilizing the natural gas-fueled SOFC–GT will likely become increasingly attractive for next-generation freight locomotives.

Acknowledgments

This material is based upon work supported under a National Science Foundation Graduate Research Fellowship. Any opinions, findings, conclusions, or recommendations expressed in this publication are those of the author and do not necessarily reflect the views of the National Science Foundation.

The statements and conclusions in this Report are those of the contractor and not necessarily those of the California Air Resources Board. The mention of commercial products, their

source, or their use in connection with material reported herein is not to be construed as actual or implied endorsement of such products.

This report was prepared as a result of work sponsored, paid for, in whole or in part, by the South Coast Air Quality Management AQMD (AQMD). The opinions, findings, conclusions, and recommendations are those of the author and do not necessarily represent the views of AQMD. AQMD, its officers, employees, contractors, and subcontractors make no warranty, expressed or implied, and assume no legal liability for the information in this report. AQMD has not approved or disapproved this report, not has AQMD passed upon the accuracy or adequacy of the information contained herein.

Appendix A. Diesel reformation reactions of Dorazio and Castaldi [51]

Reaction	A	m	E_a (kJ/kmol)
$C_{14}H_{30} + 7O_2 \leftrightarrow 15H_2 + 14CO$	5.00e46	0.0	0
$C_{14}H_{30} + 21.5O_2 \leftrightarrow 15H_2O + 14CO_2$	4.89e15	0.0	0
$C_{14}H_{30} \leftrightarrow C_7H_{16} + C_7H_{14}$	8.51e05	0.0	8.209e4
$C_{14}H_{30} + 14H_2O \leftrightarrow 29H_2 + 14CO$	9.62e56	0.0	2.170e3
$C_7H_{16} + 7H_2O \leftrightarrow 15H_2 + 7CO$	3.45e31	0.0	1.107e3
$C_7H_{14} + 7H_2O \leftrightarrow 14H_2 + 7CO$	3.76e36	0.0	9.191e2
$C_2H_4 + 2H_2O \leftrightarrow 4H_2 + 2CO$	4.96e09	0.0	2.103e2
$C_3H_6 + 3H_2O \leftrightarrow 6H_2 + 3CO$	3.28e13	0.0	3.735e2
$CH_4 + H_2O \leftrightarrow 3H_2 + CO$	7.57e07	0.0	2.061e2
$CO + H_2O \leftrightarrow H_2 + CO_2$	1.00e11	0.0	0
$C_7H_{14} + 3.5O_2 \leftrightarrow 7H_2 + 7CO$	1.26e30	0.0	0
$C_7H_{14} + 10.5O_2 \leftrightarrow 7H_2O + 7CO_2$	9.18e14	0.0	0
$C_7H_{16} + 3.5O_2 \leftrightarrow 8H_2 + 7CO$	1.77e25	0.0	0
$C_7H_{16} + 11O_2 \leftrightarrow 8H_2O + 7CO_2$	2.37e09	0.0	0
$C_7H_{16} \rightarrow C_4H_9 + C_3H_7$	1.00e40	−4.2	1.328e2
$C_4H_9 \rightarrow C_3H_6 + CH_3$	1.40e09	−0.3	3.023e1
$C_4H_9 \rightarrow C_2H_5 + C_2H_4$	1.41e09	−0.3	2.958e1
$C_3H_7 \rightarrow CH_3 + C_2H_4$	2.23e07	−0.1	1.188e2
$CH_3 + H_2O \leftrightarrow CH_4 + OH$	3.11e05	0.7	0
$CH_3 + C_2H_5 \leftrightarrow CH_4 + C_2H_4$	4.02e13	−0.1	0
$CH_3 + H_2 \leftrightarrow CH_4 + H$	5.94e05	0.7	0
$C_2H_4 + OH \leftrightarrow C_2H_3 + H_2O$	7.87e10	0.0	1.993e1
$C_2H_4 + CH_3 \leftrightarrow C_3H_6 + H$	2.10e27	−1.4	1.058e2
$C_2H_4 \leftrightarrow C_2H_3 + H$	2.96e12	0.0	3.585e2

References

[1] United States Department of the Interior. National Elevation Dataset. <http://ned.usgs.gov/>; August, 2006. (accessed 11.07.11).
[2] United States Department of Transportation: Research and Innovative Technology Administration, Bureau of Transportation Statistics. 2007 Commodity Flow Survey; 2009.
[3] United States Department of Transportation: Research and Innovative Technology Administration, Bureau of Transportation Statistics. Transportation Statistics Annual Report; 2010.
[4] Port of Long Beach. Facts at Glance. 2010. April 19, 2010. <http://www.polb.com/about/facts.asp>.
[5] Port of Los Angeles. Facts and Figures. 2009. April 19, 2010. <http://www.portoflosangeles.org/newsroom/press_kit/facts.asp>.
[6] California Air Resources Board. Diesel Particulate Matter Exposure Assessment Study for the Ports of Los Angeles and Long Beach. Sacramento; 2006.
[7] California Air Resources Board. Almanac Emission Projection Data. 2009. April 19, 2010. <http://www.arb.ca.gov/app/emsinv/emssumcat_query.php?F_YR=2008&F_DIV=-4&F_SEASON=A&SP=2009&F_AREA=CA#8>.
[8] California Air Resources Board. Health Risk Assessment for the BNSF Railway San Bernardino Railyard. Sacramento; 2008 (a).
[9] General Electric. The evolution series locomotives: moving rail power forward; 2005.
[10] Stodolsky Frank. Railroad and locomotive technology roadmap. Argonne: US Department of Energy; 2002.
[11] Jones LE, Hayward GW, Kalyanam KM, Rotenberg Y, Scott DS, Steinberg BA. Fuel cell alternative for locomotive propulsion. Int J Hydrogen Energy 1985;10:505–16.
[12] Murray HS, Huff JR, Gregory II EW. Fuel cell power plants for heavy-duty transportation applications. Extended Abstracts Electrochem Soc 1982;82:471.
[13] Steinberg BA, Scott DS. Hydrogen vs diesel fueled locomotives: a techno-economic appraisal. Int J Hydrogen Energy 1984;9(1):101–7.
[14] Kemp R. Hydrogen offers no alternative to main line electrification. Railway Gaz Int 2007:493.
[15] Scott DS, Rogner HH, Scott MB. Fuel cell locomotives in Canada. Int J Hydrogen Energy 1993;18(3):253–63.
[16] Shimada M, Furuta R, Kawasaki J, Takeda S, Kaneko T, Toyota E. Trial run of fuel cell hybrid traction system for railcar. In: Proceedings of the 23rd electric vehicle symposium. Anaheim; 2007.
[17] Hasegawa H, Ohki Y. Development of a model of on-board PEMFC powered locomotive with a metal hydride cylinder. Pittsburgh: Materials Research Society Symposia Proceedings; 1995.
[18] Jones WD. Hydrogen on track: trains and industrial equipment now, cars later. IEEE Spectrum 2006:10–3.
[19] Miller AR, Peters J. Fuel cell hybrid locomotives: applications and benefits. In: Proceedings of the 2006 IEEE/ASME joint rail conference. Atlanta; 2006.
[20] Miller AR, Peters J, Smith BE, Velev OA. Analysis of fuel cell hybrid locomotives. J Power Sources 2006;157:855–61.
[21] Miller AR, Hess KS, Barnes DL, Erickson TL. System design of a large fuel cell hybrid locomotive. J Power Sources 2007;173:935–42.
[22] Winkler W, Lorenz H. Design studies of mobile applications with SOFC-heat engine modules. J Power Sources 2002;106:338–43.
[23] Winkler Wolfgang, Lorenz H. The design of stationary and mobile solid oxide fuel cell–gas turbine systems. J Power Sources 2002;105:222–7.
[24] Martinez AS, Brouwer J, Samuelsen GS. Feasibility study of SOFC–GT hybrid locomotive: Part I. Development of a 3.5 MW SOFC–GT FORTRAN model. J Power Sources 2012;213:203–17.
[25] Martinez AS, Brouwer J, Samuelsen GS. Feasibility study of SOFC–GT hybrid locomotive: Part II. Power system packaging and operating route simulation. J Power Sources 2012;213:358–74.
[26] Schroeder DJ, Majumdar P. Feasibility analysis for solid oxide fuel cells as a power source for railroad road locomotives. Int J Hydrogen Energy 2010;35:11308–14.
[27] Guo L, Yedavalli K, Zinger D. Design and modeling of power system for a fuel cell hybrid switcher locomotive. Energy Conversion Manage 2011;52:1406–13.
[28] United States Energy Information Agency. Petroleum Navigator. April 12, 2010. April 16, 2010. <http://tonto.eia.doe.gov/dnav/pet/hist/LeafHandler.ashx?n=pet&s=ddr001&f=a>.
[29] Kang I, Kang Y, Yoon S, Bae G, Bae J. The operating characteristics of solid oxide fuel cells driven by diesel autothermal reformate. Int J Hydrogen Energy 2008;33(21):6298–307.
[30] Lawrence J, Boltze M. Auxiliary power unit based on a solid oxide fuel cell and fuelled with diesel. J Power Sources 2006;154:479–88.
[31] Lindermeir A, Kah S, Kavuruc S, Muhlner M. On-board diesel fuel processing for an SOFC-APU – technical challenges for catalysis and reactor design. Appl Catal B: Environ 2007;70:488–97.
[32] Stelter M, Reinert A, Mai BE, Kuznecov M. Engineering aspects and hardware verification of a volume producable solid oxide fuel cell stack design for diesel auxiliary power units. J Power Sources 2006;154:448–55.
[33] Yoon S, Bae, J. A diesel fuel processor for stable operation of solid oxide fuel cells system: I. Introduction to post-reforming for the diesel fuel processor. Catal Today, in press, Corrected Proof, doi: http://dx.doi.org/10.1016/j.cattod.2010.01.006.
[34] Atkinson A, Barnett S, Gorte RJ, Irvine JTS, McEvoy AJ, Mogensen M, et al. Advanced anodes for high-temperature fuel cells. Nat Mater 2004;3:17–27.
[35] Sin A, Kopnin E, Dubitsky Y, Zaopo A, Arico AS, La Rosa D, et al. Performance and life-time behavior of NiCu-CGO anodes for the direct electro-oxidation of methane in IT-SOFCs. J Power Sources 2007;164:300–5.
[36] Xie Z, Zhu W, Zhu B, Xia C. $Fe_xCo_{0.5-x}Ni_{0.5}$-SDC anodes for low-temperature solid oxide fuel cells. Electrochim Acta 2006;51:3052–7.
[37] Lu ZG, Zhu JH, Bi ZH, Lu XC. A Co–Fe alloy as alternative anodes for solid oxide fuel cell. J Power Sources 2008;180:172–5.
[38] Nikolla E, Schwank JW, Linic S. Hydrocarbon steam reforming on Ni alloys at solid oxide fuel cell operating conditions. Catal Today 2008;136:243–8.
[39] Shekhawat D, Berry DA, Haynes DJ, Spivey JJ. Fuel constituent effects on fuel reforming properties for fuel cell applications. Fuel 2009;88:817–25.
[40] Curran HJ, Gaffuri P, Pitz WJ, Westbrook CK. A comprehensive modeling study of n-heptane oxidation. Combust Flame 1998;114:149–77.
[41] Dagaut P. On the kinetics of hydrocarbons oxidation from natural gas to kerosene and diesel fuel. Phys Chem Chem Phys 2002;4:2079–94.
[42] Dobbins RA, Fletcher RA, Benner Jr BA, Hoeft S. Polycyclic aromatic hydrocarbons in flames, in diesel fuels, and in diesel emissions. Combust Flame 2006;144:773–81.
[43] Krestinin AV. Detailed modeling of soot formation in hydrocarbon pyrolysis. Combust Flame 2000;121:513–24.
[44] Vlasov PA, Warnatz J. Detailed kinetic modeling of soot formation in hydrocarbon pyrolysis behind shock waves. Proc Combust Inst 2002;29:2335–41.

[45] Come GM, Warth V, Glaude PA, Fournet R, Battin-Leclerc F, Scacchi G. Computer-aided design of gas-phase oxidation mechanisms-application to the modeling of n-heptane and iso-octane oxidation. 26th Symposium on combustion; 1996; p. 775–762.
[46] Parmar RD, Kundu A, Thurgood C, Peppley BA, Karan K. Kinetic studies of the autothermal reforming of tetradecane over Pt/Al_2O_3 catalyst in a fixed-bed reactor. Fuel 2010;89:1212–20.
[47] Amplett JC, Mann RF, Peppley BA, Roberge PR, Rodrigues A, Salvador JP. Simulation of a 250 kW diesel fuel processor/PEM fuel cell system. J Power Sources 1998;71:179–84.
[48] Cutillo A, Specchia S, Antonini M, Saracco G, Specchina V. Diesel fuel processor for PEM fuel cells: two possible alternatives (ATR versus SR). J Power Sources 2006;154:379–85.
[49] Semelsberger TA, Brown LF, Borup RL, Inbody MA. Equilibrium products from autothermal processes for generating hydrogen-rich fuel-cell feeds. Int J Hydrogen Energy 2004;29:1047–64.
[50] Specchia S, Cutillo A, Saracco G, Specchia V. Concept study on ATR and SR fuel processors for liquid hydrocarbons. Indust Eng Chem Res 2006;45:5298–307.
[51] Dorazio L, Castaldi M. Autothermal reforming of tetradecane ($C_{14}H_{30}$): a mechanistic approach. Catal Today 2008;136:273–80.
[52] GasTurb. Computer Software. Joachim Kurzke. Windows. Internet Download; 2009.
[53] Southern California Association of Governments. Regional Rail Simulation Findings Technical Appendix. 2011 January 7, 2015. <http://www.freightworks.org/DocumentLibrary/Comprehensive%20Regional%20Goods%20Movement%20Plan%20and%20Implementation%20Strategy%20-%20Regional%20Rail%20Simulation%20Findings.pdf>.
[54] Lundberg WL, Veyo SE, Moeckel MD. A high-efficiency solid oxide fuel cell hybrid power system using the mercury 50 advanced turbine systems gas turbine. J Eng Gas Turbines Power 2003;125:51–8.
[55] Caterpillar. Locomotive 3516B engine; 2000.
[56] United States Environmental Protection Agency. Technical highlights: emissions factors for locomotives. Washington, DC; 2011.
[57] Ianni, James C. Kintecus windows version 2.80, 2002. <http://www.kintecus.com>.
[58] Kawasaki. Kawasaki gas turbine generator sets; 2007.